Space Sci Rev (2020) 216:39
https://doi.org/10.1007/s11214-020-00661-2

Tidal Disruptions of White Dwarfs: Theoretical Models and Observational Prospects

Kate Maguire[1] · Michael Eracleous[2] · Peter G. Jonker[3,4] · Morgan MacLeod[5] · Stephan Rosswog[6]

Received: 17 May 2019 / Accepted: 16 March 2020 / Published online: 25 March 2020

Abstract White dwarf stars that enter the tidal radius of black holes with masses $\lesssim 10^5$ $M_\odot$ are doomed to be ripped apart by tidal forces. Black holes in this mass range between stellar black holes and supermassive black holes have not been conclusively identified so the detection of a tidal disruption of a white dwarf would provide clear evidence for the existence of intermediate-mass black holes. In this review, we present a theoretical and observational overview of the transient events that result from the tidal disruptions of white dwarfs by intermediate-mass black holes. This includes discussion of the latest simulations and pre-

The Tidal Disruption of Stars by Massive Black Holes
Edited by Peter G. Jonker, Sterl Phinney, Elena Maria Rossi, Sjoert van Velzen, Iair Arcavi and Maurizio Falanga

✉ K. Maguire
kate.maguire@tcd.ie

M. Eracleous
mxe17@psu.edu

P.G. Jonker
p.jonker@astro.ru.nl

M. MacLeod
morgan.macleod@cfa.harvard.edu

S. Rosswog
stephan.rosswog@astro.su.se

1 School of Physics, Trinity College Dublin, The University of Dublin, College Green, Dublin 2, Ireland

2 Department of Astronomy & Astrophysics and Institute for Gravitation and the Cosmos, The Pennsylvania State University, 525 Davey Lab, University Park, PA 16802, USA

3 SRON, Netherlands Institute for Space Research, Sorbonnelaan 2, 3584 CA, Utrecht, The Netherlands

4 Department of Astrophysics/IMAPP, Radboud University Nijmegen, P.O. Box 9010, 6500 GL, Nijmegen, The Netherlands

5 Harvard-Smithsonian Center for Astrophysics, 60 Garden Street, MS-51, Cambridge, MA 02138, USA

dicted properties, the results of observational searches, as well as a summary of the potential for gravitational wave emission to be detected with upcoming missions.

Keywords White dwarf · Intermediate-mass black hole

1 Introduction

White dwarfs are the final products of the evolution of low-mass stars. They result from stars between ~ 0.1–8 $M_\odot$ that are not massive enough to ignite further burning stages of their helium or carbon-oxygen cores. Thus, these cores cool and evolve into very dense stars ($\sim 10^6$ g cm^{-3}) whose masses are determined by their baryon content, but the pressure necessary to maintain hydrostatic equilibrium is provided by the fermionic "degeneracy pressure" of their electrons. While under normal circumstances this is the end of their nuclear evolution, at least in principle, much more nuclear energy can be gained by transforming the white dwarfs (7.08 MeV/nucleon for helium, 7.68 MeV/nucleon for carbon, and 7.98 MeV/nucleon for oxygen) into iron group elements (8.79 MeV/nucleon): ~ 1 MeV/nucleon or $\sim 2 \times 10^{51}$ erg/$M_\odot$ can still be released. Perhaps the most spectacular way to trigger this release, is to send the white dwarf close a black hole (BH) and explosively ignite it by tidal compression (Luminet and Pichon 1989; Rosswog et al. 2009).

White dwarfs have typical sizes comparable to the Earth's, but following an inverted mass-radius relation they are smaller the more massive they are, as depicted in Fig. 1. Using a convenient analytic expression derived by Nauenberg (1972, see also Appendix A of Even and Tohline 2009), we can cast the mass-radius relation of a Carbon-Oxygen white dwarf as

$$R_{\rm wd} = 7.80 \times 10^8 \left(\frac{M_{\rm wd}}{M_{\rm Ch}}\right)^{-1/3} \left[1 - \left(\frac{M_{\rm wd}}{M_{\rm Ch}}\right)^{4/3}\right]^{1/2} \ {\rm cm} \tag{1}$$

where $M_{\rm Ch} = 1.435$ $M_\odot$ is the Chandrasekhar mass for that composition. This mass-radius relation, plotted in Fig. 1, is the reason why the average density of white dwarfs rises sharply with increasing mass, as shown by the red curve in Fig. 1.

BHs are usually classified according to their masses. The existence of stellar mass BHs ($\lesssim 60$ $M_\odot$) and supermassive BHs ($\sim 10^6$–10^{10} $M_\odot$; SMBHs) is well established, but members with masses between these two regimes, so-called intermediate-mass BHs (IMBHs), have not been conclusively identified. They are thought to form via a variety of physical mechanisms, e.g., runaway stellar collisions in a dense star cluster and collapse of a massive gas cloud (see, for example, Portegies Zwart and McMillan 2002; Begelman et al. 2008; Mayer et al. 2010).

To be torn apart by the tidal forces of a BH, a white dwarf must come closer than the tidal radius

$$R_{\rm t} \simeq R_{\rm wd} \left(\frac{M_\bullet}{M_{\rm wd}}\right)^{1/3}. \tag{2}$$

For an accretion disk to form around the BH, the disruption needs to occur outside the innermost stable circular orbit at $R_{\rm ISCO,S} = 6GM_\bullet/c^2 \equiv 6R_{\rm g}$ for a Schwarzschild BH or $R_{\rm ISCO,eK} = R_{\rm g}$ for a maximally rotating Kerr BH and a prograde orbit ($R_{\rm g}$ is conventionally

6 Department of Astronomy & Oskar Klein Centre, Stockholm University, AlbaNova, Roslagstullbacken 21, 10691 Stockholm, Sweden

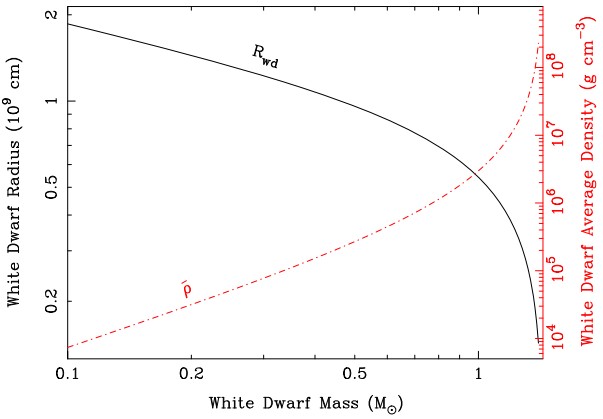

Fig. 1 Radius of a Carbon-Oxygen white dwarf as a function of its mass (in $M_\odot$). The mass-radius relation of equation (1) is adopted here, which is due to Nauenberg (1972). For reference, the red dot-dashed line (labelled $\bar{\rho}$ with corresponding scale on the right) shows the average density of the white dwarf as a function of its mass

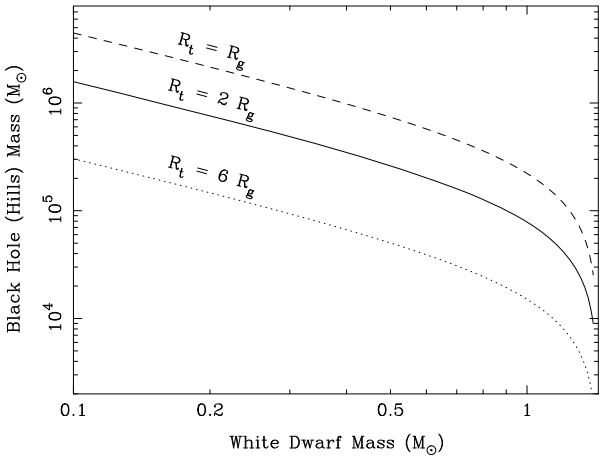

Fig. 2 The variation of the BH Hills mass with white dwarf mass. The three curves represent the boundaries below which the white dwarf is disrupted outside of the innermost stable circular orbit of a non-rotating BH (dotted line, labelled $R_t = 6R_g$), the event horizon of a non-rotating BH (solid line, labelled $R_t = 2R_g$) and the event horizon of a maximally-rotating BH, which is also its innermost stable circular orbit (dashed line, labelled $R_t = R_g$). The curves are obtained by equating the tidal disruption radius with the appropriate horizon radius and rearranging the equation to express the BH mass in terms of the white dwarf mass

referred to as the gravitational radius). If the tidal radius lies inside the event horizon ($R_{H,S} = 2R_g$ for the Schwarzschild and $R_{H,eK} = R_g$ for the extreme Kerr case), no disruption occurs and the white dwarf is "swallowed" whole. These thresholds are plotted as a function of the white white dwarf mass in Fig. 2. Since the tidal radius is proportional to $M_\bullet^{1/3}$, but the other radii are proportional to $M_\bullet$, there is a (spin-dependent) upper limit on the BH mass beyond which tidal disruption events (TDEs) are impossible. For a non-rotating black hole and a white dwarf of typical mass ($\approx 0.6\ M_\odot$; Kepler et al. 2007), this limiting BH mass is $\sim 2 \times 10^5\ M_\odot$, therefore only IMBHs can disrupt white dwarfs, see Fig. 2.

The strength of a tidal encounter is often quantified by the parameter $\beta \equiv R_t/R_p$, i.e., the inverse ratio of the pericentre distance to the tidal disruption radius. In other words, a strong encounter is one where the white dwarf penetrates deeply into the tidal radius. Figure 3

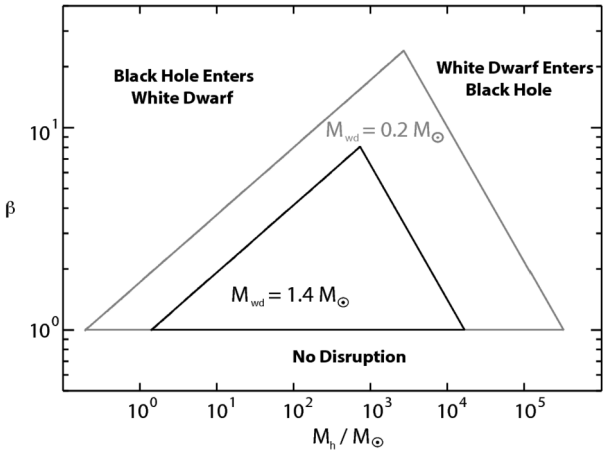

Fig. 3 The parameter space defined by the strength of the tidal encounter ($\beta \equiv R_t/R_p$) and the BH mass, M_h (assuming a non-rotating BH). This particular figure shows the interesting regions of the diagram for a 1.4 $M_\odot$ and a 0.2 $M_\odot$ white dwarf and was taken from Rosswog et al. (2009); an earlier version illustrating the same regions for a 0.6 $M_\odot$ white dwarf was shown by Luminet and Pichon (1989). In the lower region of the diagram, where $\beta < 1$, there is no disruption. If the combination of β and M_h falls within the triangle corresponding to the white dwarf's mass, the white dwarf is disrupted outside the event horizon of the BH and the post-disruption debris eventually returns to pericentre. In the upper right corner of the diagram the disruption occurs within the event horizon of the BH. In the upper left corner of the diagram, the black hole event horizon is smaller than the white dwarf, therefore the BH effectively enters the white dwarf during a strong encounter

illustrates the outcome of a tidal encounter in the β–$M_\bullet$ plane for two different white dwarf masses. For $\beta < 1$ there is no disruption since the white dwarf does not cross the tidal disruption radius. For a given white dwarf mass, the triangle encompasses the region of this parameter space where the debris eventually returns to pericentre after disruption; some of this debris can be subsequently accreted by the BH. For strong encounters outside of this triangle, the BH either enters the white dwarf or it "swallows" the white dwarf whole.

The most promising TDE locations depend on the type of disruption. TDEs of main sequence stars by SMBHs are associated with the cores of galaxies where SMBHs are generally found. However, TDEs involving white dwarfs and IMBHs may occur in a more diverse range of environments since IMBHs are predicted to occur in dwarf galaxies (e.g., Reines et al. 2013), globular clusters (Jonker et al. 2012) and in hyper-compact stellar clusters (Merritt et al. 2009), although the predicted rates for these different environments differ enormously. The discovery of a transient caused by the tidal disruption of a white dwarf by a BH would be clear evidence for the existence of an IMBH. Such a discovery would be extremely interesting for a variety of reasons:

1. IMBHs are routinely invoked as "seeds" in scenarios for the growth of SMBHs and their co-evolution with their host galaxies (see, for example, the review by Volonteri 2012). Seed masses of at least 10^3 $M_\odot$ are required in order to explain the large BH masses found in the highest-redshift quasars (e.g. Mortlock et al. 2011; Fan 2006; Bañados et al. 2018, these black holes must have grown to $\sim 10^9$ $M_\odot$ in ~ 700 Myr by Eddington-limited accretion).
2. Dwarf galaxies (with stellar masses $M_* \lesssim 10^9$ $M_\odot$) are the expected hosts of IMBHs based on an extrapolation of the relation between BH mass and host galaxy stellar

spheroid mass (e.g., McConnell and Ma 2013) and on the identification of active galactic nuclei (AGNs) in many dwarf galaxies (e.g., Reines et al. 2013; Moran et al. 2014; Baldassare et al. 2018). But the occupation fraction, which is critical in setting the white dwarf TDE rate is unknown. Circumstantial arguments by Silk (2017) suggest that an occupation fraction near unity would resolve many of the open questions in dwarf galaxy evolution.

3. Observations of flares from white dwarf disruptions would afford useful tests of models for the accretion of Hydrogen deficient matter at very high rates relative to the Eddington limit (e.g., Dai et al. 2018), the formation of jets (e.g., Krolik and Piran 2012), and the transition from super- to sub-Eddington flows. Since the BH mass is relatively low in this case, the Eddington ratio (accretion rate divided by the Eddington rate) will be much higher than in the disruption of normal stars by more massive BHs and the accretion flow will evolve on a considerably shorter time scale.
4. The event *rates* afford important tests of models for the stellar populations and dynamics in the vicinity of the BH. Since the expected rate estimates depend on a number of assumptions, as we detail later in this chapter, one could potentially eliminate entire families of models based on measurements of the event rates, which would represent substantial progress.
5. White dwarfs in bound orbits spiraling into IMBHs can produce a detectable gravitational wave signal before disruption (e.g., Sesana et al. 2008). From this signal we can potentially infer many of the fundamental properties of the system, including the masses of the white dwarf and IMBH, which is extremely useful for testing models of the post-disruption accretion flow (discussed further in Sect. 7.1, below, and in other chapters in this volume).

One can appreciate the importance of general relativistic effects during such disruptions by expressing the tidal disruption radius in units of the gravitational radius. Combining equation (2) with the definition of β and $R_{\rm g}$ one can write

$$\frac{R_{\rm p}}{R_{\rm g}} = \frac{R_{\rm t}}{\beta R_{\rm g}} \simeq \frac{80}{\beta}\left(\frac{R_{\rm WD}}{10^9\ {\rm cm}}\right)\left(\frac{M_{\rm wd}}{0.6\ {\rm M}_\odot}\right)^{-1/3}\left(\frac{M_\bullet}{10^3\ {\rm M}_\odot}\right)^{-2/3}. \tag{3}$$

Thus, a strong encounter of a typical white dwarf with a 10^4 $\rm M_\odot$ BH can have $R_{\rm p}/R_{\rm g} < 10$, i.e., the white dwarf gets within 5 Schwarzschild radii of the BH during its initial fly-by. Such an encounter is relativistic.

The aim of this chapter is to discuss the theoretical and observational properties of the transients that result from the tidal disruptions of white dwarfs by IMBHs. In Sect. 2, the underlying theory and simulations necessary for analysing these interactions are highlighted. In Sect. 3, the predicted nucleosynthetic yields of systems that result in the detonation of the white dwarf are discussed, while in Sect. 4 the expected optical and UV signatures of white-dwarf tidal-disruption events (TDEs) are highlighted. In Sect. 5, observational searches for the tidal disruptions of white dwarfs and candidate events are described. The intrinsic and predicted rates of white dwarf TDEs are detailed in Sect. 6. A summary of the expected gravitational wave emission from the tidal disruptions of white dwarfs by IMBHs and the cosmic ray acceleration in ensuing jets is provided in Sect. 7.

2 Theory and Simulations

Some aspects of TDEs can be described to good accuracy in a purely analytical way (Luminet and Marck 1985; Luminet and Carter 1986; Rees 1988; Stone et al. 2013), but in

reality a TDE is a highly non-linear interaction between gravity (both self-gravity of the star and the "background" gravity from the BH), gas dynamics, radiation, potentially magnetic fields and – in extreme cases – thermonuclear reactions. Therefore, most astrophysically relevant questions need to be addressed via careful numerical simulations.

2.1 Geometrical Challenges

The lengths and timescales involved make TDEs formidable numerical challenges and prevent, in particular for most realistic cases, the "just-do-it" approach, where the Einstein and hydrodynamics equations are solved together in a consistent way.

The initial star far from the BH is in hydrostatic equilibrium between gas pressure gradients and self-gravity. The acceleration from self-gravity is $a_{\rm sg} \sim GM_{\rm wd}/R_{\rm wd}^2$, while the tidal acceleration at a distance d from the BH is $a_{\rm tid} \sim GM_\bullet R_{\rm wd}/d^3$, so that their ratio is

$$\frac{a_{\rm tid}}{a_{\rm sg}} \sim \left(\frac{M_\bullet}{M_{\rm wd}}\right)\left(\frac{R_{\rm wd}}{d}\right)^3 \equiv \left(\frac{R_t}{d}\right)^3, \tag{4}$$

which implies, not too surprisingly, a ratio of unity at the tidal radius given by Eq. (2). Equation (4) shows further that for the tidal acceleration to be a $< 1\%$ perturbation of the stellar equilibrium, the initial separation, d_0, for starting a numerical simulation needs to be at least

$$d_0 \sim 5R_t, \tag{5}$$

making the initial star a tiny fraction of the simulation volume:

$$\left(\frac{R_{\rm wd}}{d_0}\right)^3 \sim 10^{-8}\left(\frac{M_{\rm wd}}{1\ {\rm M}_\odot}\right)\left(\frac{10^6\ {\rm M}_\odot}{M_\bullet}\right). \tag{6}$$

This is only dependent on the mass ratio and actually independent of the radius of the star that is disrupted. Therefore, the challenge is alleviated for an IMBH-white dwarf disruption compared to one where a main sequence star is disrupted by a SMBH. Equation (6) has repercussions for simulating TDEs. While the small volume covered by the initial star does not pose any challenge for a Lagrangian method like smooth particle hydrodynamics (SPH; Monaghan 2005; Rosswog 2009; Springel 2010; Rosswog 2015), it is a serious hurdle for Eulerian methods, where vacuum has to be treated as a low-density background gas that must be evolved during the simulation. Therefore, such simulations are often performed in the reference frame of the stellar centre of mass, with the BH being treated as a time-varying, external force (Guillochon et al. 2009; Guillochon and Ramirez-Ruiz 2013). This reduces the computational volume and avoids excessive numerical advection error due to high velocity motion of the gas with respect to the computational grid.

2.2 Hydrodynamics and Gravity Challenges and Approaches

Additional simulation challenges come from restriction of the numerical time step. For a full space-time solution approach, the relevant signal velocity that enters the Courant-Friedrichs-Lewy stability criterion (Courant et al. 1928) is the speed of light, so that the numerical time step is restricted to

$$\Delta t < 10^{-3}\ {\rm s}\left(\frac{\Delta x}{3\times 10^7\ {\rm cm}}\right), \tag{7}$$

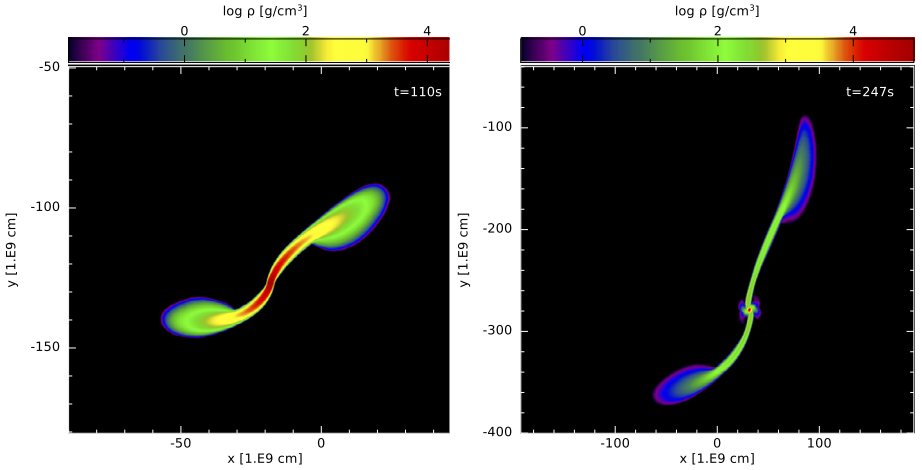

Fig. 4 Partial tidal disruption of a 0.5 $M_\odot$ white dwarf by a 1000 $M_\odot$ BH (located at the coordinate origin) illustrating a weak encounter with an impact parameter $\beta = 0.8$ (Rosswog 2019). The star is "almost completely" disrupted (left panel), but a small self-gravitating core survives within the tidal stream connecting the two tidal lobes (right panel). The simulation started at an initial separation of $5R_t$

where Δx is the resolution length and its numerical value for the scaling has been chosen so that it corresponds to resolving a typical white dwarf radius with ~ 30 resolution lengths. Self-gravity of the stellar material can play a decisive role since it, together with the BH's tidal field, determines the density structure inside the star. Since nuclear reactions are very sensitive to matter density, self-gravity is crucial for an accurate modeling of a possible explosion. For weak encounters with $\beta \lesssim 1$, also partial disruptions can occur where the star is "nearly disrupted", but its original stellar core collapses again under its own gravitational pull. Such a situation is illustrated in Fig. 4 for a 0.5 $M_\odot$ white dwarf, a 1000 $M_\odot$ BH and a penetration factor $\beta = 0.8$. Such surviving cores can have an impact on the debris properties and subsequent fallback rates (Guillochon and Ramirez-Ruiz 2013). This illustrates the serious challenge of full end-to-end simulations where a star approaches the BH from a large distance, becomes disrupted when passing the BH into a thin gas stream with a potentially self-gravitating stellar core, and returns later to the BH vicinity to finally settle into an accretion disk. Thus full space-time solution approaches are limited to the near-neighbourhood of the BH.

To date, the following strategies have been followed in numerical TDE simulations:

a) use an entirely Newtonian approach and restrict the focus to encounters that can be treated as non-relativistic with a reasonable accuracy (e.g. Guillochon and Ramirez-Ruiz 2013; Guillochon et al. 2014; Coughlin and Nixon 2015; Goicovic et al. 2019);
b) use Newtonian numerical hydrodynamics together with a pseudo-Newtonian potential for approximately capturing some relativistic effects (Rosswog et al. 2009; Tejeda and Rosswog 2013; Hayasaki et al. 2013; Bonnerot et al. 2015; Gafton et al. 2015);
c) follow a post-Newtonian approach for mildly relativistic encounters (Ayal et al. 2000, 2001; Hayasaki et al. 2016);
d) use relativistic hydrodynamics in a fixed BH space time, but neglect the self-gravity of the star (e.g. Anninos et al. 2018);
e) like d), but adding Newtonian self-gravity of the star (Kobayashi et al. 2004; Rantsiou et al. 2008);

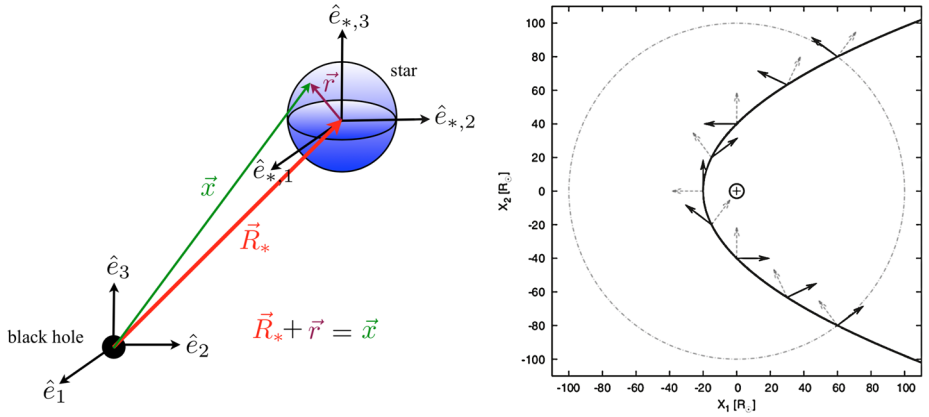

Fig. 5 Left: Reference frames used for the analysis of the tidal action of a BH on a star with quantities as discussed in Sect. 2.3. Right: Eigenvectors of the tidal tensor (shown as arrows), taken from Brassart and Luminet (2008). The circle indicates the tidal radius, the parabola the stellar orbit, the BH position is indicated by the cross. The third eigendirection (not shown) is perpendicular to the orbital plane

f) use a full numerical relativity approach by solving the Einstein equations, and restrict the attention mainly to regions near the BH (e.g. Haas et al. 2012; East 2014; Evans et al. 2015)); surviving stellar cores (as seen in Fig. 4) in partial disruptions pose a very serious challenge to such an approach;
g) use a combination of some of the above approaches, e.g. follow the gas motion far from the BH with Newtonian methods and near the BH with relativistic hydrodynamics similar to approach d) (e.g. Shiokawa et al. 2015; Sądowski et al. 2016);
h) start from a Kerr metric, but include the stellar (WD) contributions to the scalar curvature components in the metric (Anninos et al. 2019) to approximate the stellar self-gravity. This (expensive) correction is switched-off close to the black hole.
i) use the Newtonian hydrodynamics equations as the computational core, but "wrap them" into functions that contain the BH metric and its derivatives (Tejeda et al. 2017; Gafton and Rosswog 2019); this method very accurately reproduces fully relativistic approaches and includes the self-gravity of the star/its debris.

2.3 Black Hole Tides Deforming a Nearby Star

It is instructive to study how the tidal forces from a BH distort a star. As a first approximation assume that the BH can be reasonably described as a Newtonian point mass. Further assume that a coordinate system with unit vectors $\{\hat{e}_1, \hat{e}_2, \hat{e}_3\}$ is attached to the BH and another coordinate system is centred on the star with unit vectors $\{\hat{e}_{*,1}, \hat{e}_{*,2}, \hat{e}_{*,3}\}$, as sketched in Fig. 5. The center of mass of the star is displaced from the BH by $\vec{R}_*$ and we are interested in some location inside the star, displaced from the stellar center of mass by $\vec{r}$ and from the BH by $\vec{x} = \vec{R}_* + \vec{r}$. With these assumptions, the BH gravitational potential is

$$\Phi(\vec{x}) = -\frac{GM_\bullet}{x}, \tag{8}$$

where $x = |\vec{x}|$.

For a point $\vec{x} = \vec{R}_* + \vec{r}$ inside the star, Φ can be expanded around $\vec{R}_*$ into

$$\Phi(\vec{x}) = \Phi(\vec{R}_*) + (\partial_i \Phi)_{\vec{R}_*} r_i + \frac{1}{2}(\partial_{ij}\Phi)_{\vec{R}_*} r_i r_j + \frac{1}{6}(\partial_{ijk}\Phi)_{\vec{R}_*} r_i r_j r_k + O(r^4) \tag{9}$$

$$= \Phi(\vec{R}_*) + (\partial_i \Phi)_{\vec{R}_*} r_i + \Phi_{\rm tid}(\vec{x}). \tag{10}$$

where $\Phi_{\rm tid}$ is the tidal potential. $\Phi_{\rm tid}$ can be further split up making use of the tidal tensor (note the sign convention)

$$\tau_{ij} = -(\partial_{ij}\Phi)_{\vec{R}_*} \tag{11}$$

and the deviation tensor

$$\Delta_{ijk} = -(\partial_{ijk}\Phi)_{\vec{R}_*}. \tag{12}$$

The deviation tensor governs the deviation of the centre of mass from a pure point mass orbit and it can be shown that

$$M_* \frac{d^2 R_{*,i}}{dt^2} = -M_* \partial_i \Phi(\vec{R}_*) + \frac{1}{2}\Delta_{ijk} \int r_j r_k \rho(\vec{r}) d^3 r + O(r^3). \tag{13}$$

Since $R_* \gg r$ the deviations from a point particle orbit are usually negligibly small. The acceleration in the reference frame of the star is then given by

$$\frac{d^2 r_i}{dt^2} = \tau_{ij}(\vec{R}_*)\, r_j \tag{14}$$

and it is, therefore, the tidal tensor τ_{ij} given by Eq. (11) that determines how the star is deformed by the BH. An eigenvector analysis of τ_{ij} delivers two negative and one positive eigenvalue, i.e. the star is compressed in two eigendirections and stretched in the third. Two eigendirections (one positive, one negative) lie in the orbital plane and change as the star approaches the BH, see Fig. 5 (taken from Brassart and Luminet (2008)). The third eigendirection, with negative eigenvalue, is perpendicular to the orbital plane. Thus, as the star approaches the BH it becomes compressed in the direction perpendicular to the orbital plane.

For relativistic BHs, an equation very similar to Eq. (14) is found, with the relativistic tidal tensor, $\tau_{ij}^{\rm GR}$, containing the Riemann curvature tensor. For explicit expressions in Schwarzschild space-time, see, e.g., Brassart and Luminet (2010), Cheng and Evans (2013), and Gafton et al. (2015).

2.4 Nuclear Energy Generation

Triggering dynamically important nuclear burning processes during a TDE is non-trivial since nuclear reactions are often inefficient and the compression time during the flyby is very short (Rosswog et al. 2009). An estimate of the compression time, $\tau_{\rm comp}$, can be made assuming the white dwarf is being squeezed with freefall velocity through a point of maximum compression ("nozzle") along its orbit:

$$\tau_{\rm comp} \sim \frac{R_{\rm wd}}{v_p} \sim 0.2\ {\rm s} \left(\frac{M_{\rm wd}}{0.6\ {\rm M}_\odot}\right)^{-1/6} \left(\frac{R_{\rm wd}}{10^9\ {\rm cm}}\right)^{3/2} \left(\frac{M_\bullet}{10^3\ {\rm M}_\odot}\right)^{-1/3}, \tag{15}$$

where the orbital velocity at periastron, $v_{\rm p}$, is

$$v_{\rm p} \sim c \left(\frac{R_{\rm g}}{R_t}\right)^{1/2} \simeq 5 \times 10^9 \,{\rm cm\,s^{-1}} \left(\frac{M_{\rm wd}}{0.6\,{\rm M}_\odot}\right)^{1/6} \left(\frac{R_{\rm wd}}{10^9 {\rm cm}}\right)^{-1/2} \left(\frac{M_{\rm BH}}{10^3\,{\rm M}_\odot}\right)^{1/3}. \quad (16)$$

A simple order of magnitude estimate for the conditions needed to explode a white dwarf comes from the requirement that the nuclear energy injection time scale $\tau_{\rm nuc} \equiv \epsilon_{\rm nuc}/\dot{\epsilon}_{\rm nuc}$ must be shorter than the crossing time of the star through periastron, $\tau_{\rm passage}$, so that a substantial amount of nuclear energy can be released during the short compression time. The burning time scale also has to be substantially shorter than the dynamical time scale of the star, $\tau_{\rm dyn} = 1/\sqrt{G\bar{\rho}_{\rm wd}}$, where $\bar{\rho}_{\rm wd}$ is the average white dwarf density, otherwise the star has time to react on the energy release, can expand and quench the burning. The time to pass the BH at R_t, however, is comparable to the dynamical timescale of the star,

$$\tau_{\rm passage} \sim \frac{R_t}{v_{\rm p}} \sim \frac{1}{\sqrt{G M_{\rm wd}/R_{\rm wd}^3}} \sim \tau_{\rm dyn}, \quad (17)$$

so that both conditions can be summarized as $\tau_{\rm nuc} \ll \tau_{\rm dyn}$.

2.5 Disk Formation

The formation of an accretion disk out of the disruption debris is thought to be crucial for the electromagnetic appearance of a TDE. This process, however, is to date only incompletely understood, see Chap. "Formation of an Accretion Flow" of this book. It is, in particular, not obvious that the actual accretion rate, $\dot{M}_{\rm acc}$, should, in all cases, follow the mass delivery/fallback rate, $\dot{M}_{\rm fb} \propto t^{-5/3}$, that is found from simple analytical arguments and numerical simulations (Rees 1988; Phinney 1989; Evans and Kochanek 1989; Ramirez-Ruiz and Rosswog 2009; Lodato et al. 2009; Lodato and Rossi 2011; Kesden 2012; Cheng and Bogdanović 2014). For this to be true, matter must be accreted faster than it is delivered by fallback. The disk formation process depends on the relative efficiencies of circularization, viscous accretion and radiative cooling (Evans and Kochanek 1989). All of these topics currently bear a large degree of uncertainty. The self-crossing of the accretion stream can be efficient in circularizing the disruption debris into a disk-structure (of some type). It can occur for at least two reasons. First, the debris that passes the black hole has a wide range of specific energies across the stream width which translates into a "fan" spread over a range of apocentre distances (see Rees 1988; Kochanek 1994). This fan can collide and shock with the matter falling towards the black hole, as depicted in Fig. 6. Second, if strong, relativistic apsidal precession can lead to stream self-crossing with enhanced collision angles and thus efficiently circularize the debris (Bonnerot et al. 2015; Shiokawa et al. 2015; Hayasaki et al. 2016). The apsidal precession angle is approximately given by e.g. Hobson et al. (2006) and Chap. "Formation of an Accretion Flow" in this book,

$$\Delta\Phi \approx \frac{3\pi R_g}{R_p} \approx 11.5^\circ \beta \left(\frac{M_h}{10^6\,{\rm M}_\odot}\right)^{2/3} \quad (18)$$

and therefore, is particularly pronounced for high-mass black holes.

Guillochon and Ramirez-Ruiz (2015) used an approximate scheme with Post-Newtonian orbital prescriptions to study the disruption of stars by spinning black holes via a Monte Carlo approach. For cases with strong relativistic effects and substantial black hole spins,

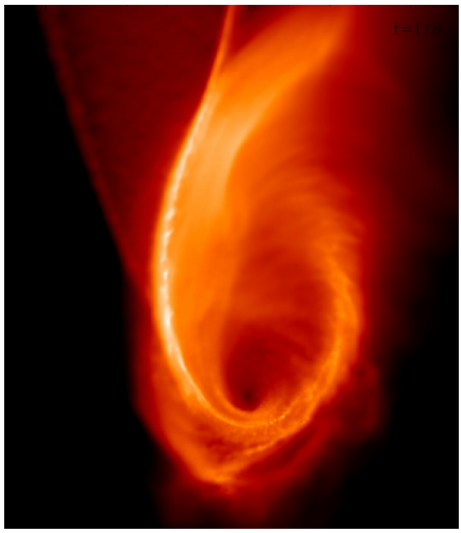

Fig. 6 The debris stream passing the black hole spreads into a "nozzle" of large apocentre distance spread. On interacting with the infalling stream a circularization shock can form. Figure from the simulations of Rosswog et al. (2009)

they found that spin-induced precession can avoid stream collisions for the times corresponding to ∼10 orbital windings resulting in some cases in substantial "dark periods" directly after the disruptions.

They find that for cases where GR effects and precession angles are small, the streams typically self-intersect far away from the black holes. This leads to long viscous time scales that can slow down the accretion rate $\dot{M}_{\rm acc}$ compared to the fallback rate $\dot{M}_{\rm fb}$ by large factors. Their Monte Carlo studies suggest that this is mostly the case for smaller black hole masses. Cases with very long viscous time scales may only peak years after the disruption with bolometric luminosities decaying more slowly than the $t^{-5/3}$-behaviour that is often used to observationally identify TDEs. Therefore such events may have gone unnoticed.

Specifically since WDs are disrupted by IMBHs, it is currently unclear if, and in which region of the parameter space, cases with very long viscous time scales occur. This is because we have on the one hand small apsidal precession angles, see Eq. (18), but on the other hand the low black hole masses favour widely spreading "fans." This interesting question is left for future explorations.

3 Nucleosynthetic Predictions of Detonations

The tidal disruptions of white dwarfs differ from those of main sequence stars in that there can be an additional source of energy: the tidal compression during the pericentre passage can trigger thermonuclear runaway reactions (e.g. Luminet and Pichon 1989; Rosswog 2009; MacLeod et al. 2016b; Kawana et al. 2017; Tanikawa et al. 2017; Anninos et al. 2018; Tanikawa 2018a). Obviously, it is easier to ignite a He-WD than one with a CO-composition. It should be mentioned, however, that a WD below $\approx 0.46\ {\rm M}_\odot$ consists of a helium core engulfed in a hydrogen envelope that can extend to several core radii and therefore increase the effective tidal radius (Law-Smith et al. 2017). Alternatively tidal compression could trigger a detonation first in a He-shell on the surface of a white dwarf followed by detonation of a CO core, 'tidal double detonation' (Tanikawa 2018b).

The first three-dimensional hydrodynamic calculations involving a nuclear network were performed in 2009 (Rosswog et al. 2009) for the tidal disruption of white dwarfs by IMBHs.

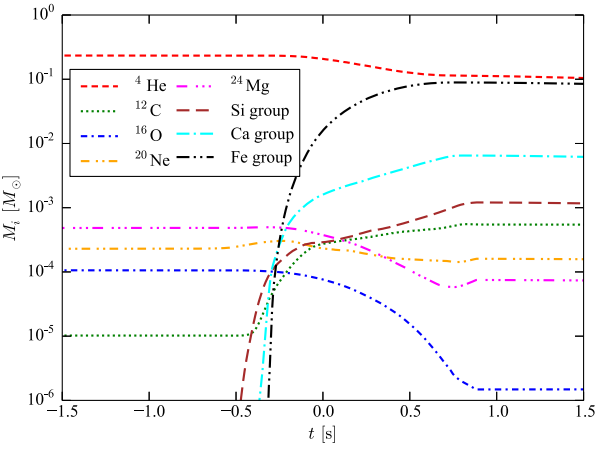

Fig. 7 The mass evolution of nuclear species for simulations B3M2R09 (a 0.2 $M_\odot$ white dwarf and 10^3 $M_\odot$ BH with a β parameter of 11). Figure from Anninos et al. 2018

These simulations used up to 4×10^6 SPH particles and each particle solved a small nuclear reaction network (Hix et al. 1998). For deep encounters ($\beta > 3$) the released nuclear energy was found to exceed the white dwarf gravitational binding energy and to lead to an explosion (Rosswog et al. 2009; Anninos et al. 2018). A recent, systematic study (Gafton and Rosswog (2019), their Fig. 17; though focussing on disruptions of main sequence stars by SMBHs) showed that for $\beta > 3$ a large fraction of the star becomes shocked via the tidal compression described in Sect. 2.3, thus supporting the idea that the explosion is triggered by compression shocks.

Reactive flows, however, are notoriously difficult numerical problems, see the excellent review of Müller (1998). The energy release from nuclear reactions creates pressure gradients that trigger fluid motions, which again transport both fuel and ashes to and from the reaction region. In the case of detonations these regions are intrinsically three-dimensional and one needs to resolve tiny length and time scales. Tanikawa et al. (2017) recently suggested that a spatial resolution of $< 10^6$ cm (with likely $> 10^9$ particles in SPH simulations) is needed to determine if explosive burning will occur. While small nuclear reaction networks can provide an accurate estimate for the nuclear energy release, and thus guarantee a reliable dynamical evolution of the fluid, substantially larger networks are needed in a post-processing step to reliably predict nucleosynthetic yields.

The relative yields of intermediate and heavy elements depend on the density during the burning processes, iron-group elements typically require densities $\gtrsim 10^7$ g cm^{-3}. Such densities can be reached by a combination of the initial stellar mass (translating into initial density and chemical composition), the β parameter (strength of the interaction) and the BH mass (Kawana et al. 2017; Tanikawa et al. 2017; Anninos et al. 2018). In particular low-mass white dwarfs need very strong encounters to potentially produce iron group elements. Figure 7 shows the nucleosynthetic production as a function of time for a general relativistic calculation of the ignition of a 0.2 $M_\odot$ He white dwarf by approach to a BH with a mass of 10^3 $M_\odot$ and β of 11. For this model, both Fe-group and intermediate-mass elements are produced. Interestingly, the black hole spin does not have much (if any) impact on the nucleosynthesis (Anninos et al. 2019).

Some observed Ca-rich transients have been suggested to originate from the tidal disruption of white dwarf by a IMBH and it is found that Ca-rich debris can be produced for low β systems. These systems, however, also have a low burning efficiency, which results

in low yields of intermediate-mass elements and so may not produce enough Ca to be the progenitors of Ca-rich transients (Kawana et al. 2017; Anninos et al. 2018).

4 Predicted Optical and UV Signatures

The tidal disruption of a white dwarf by an IMBH results in a number of separate processes that can produce observational signatures. The disruption of white dwarf material typically results in super-Eddington accretion rates which may go along with jet formation in a manner analogous to the tidal disruption of main-sequence stars. Unlike main sequence stellar disruptions, however, very strong encounters can trigger runaway nuclear burning during the first stellar passage when the star is compressed and shocked as explained in Sect. 2. This can launch a Type Ia supernova-like event, but with highly asymmetric outflow.

The early-time optical and UV spectra are expected to be featureless because of a very large electron scattering opacity in the super-Eddington outflow at this early phase (Strubbe and Quataert 2011; Roth et al. 2016). Depending on the geometry and thermal and ionization structure of the outflowing envelope, some emission and/or absorption lines may be discernible in the spectra but these are expected to fall primarily in the far-UV and soft X-ray bands. The models of Strubbe and Quataert (2011), for example, consider the transfer of continuum photons through the outflowing envelope and predict an absorption-line spectrum. The models of Roth et al. (2016) consider the random walk of continuum and emission-line photons through the envelope and predict a spectrum with a combination of emission and absorption lines that depends on the particular conditions; some of the easily discernible lines may be in the rest-frame optical part of the spectrum. Although specific calculations of the spectra from the early stages of the disruption of a white dwarf have not been carried out, we can draw an analogy with the work on main sequence stars described above. Thus we expect the rest-frame optical continuum to be largely featureless while some strong absorption lines or P-Cygni lines from elements that are abundant in a white dwarf will show up in the far-UV portion of the spectrum.

At later stages of the disruption event, i.e., after the accretion rate drops below the Eddington limit and, presumably, a conventional accretion disk forms, we may expect to see broad emission lines from the tail of returning debris. Clausen and Eracleous (2011) calculated the optical and near-UV emission-line spectrum from the photoionized debris tail and its evolution over 11 years by adopting and refining the methodology of Strubbe and Quataert (2009). They considered a 0.55 $M_\odot$ CO white dwarf (67% O, 32% C, and 1% He by mass)[1] disrupted by IMBHs of 10^2, 10^3, and 10^4 $M_\odot$ with encounter strengths of $\beta = 1$ and 3.3. They found that, the (permitted) C IV λ1550 and C III λ977 Å lines are the two brightest lines in the spectrum and that their strengths decline monotonically with time as the event evolves. During the sub-Eddington accretion rate phase, the strengths of these two lines decline *approximately* as $t^{-5/3}$, mirroring the assumed decay rate of the ionizing luminosity. The strongest lines in the rest-frame optical spectra are the (forbidden) [O III] $\lambda\lambda$4959,5007 and [O III] λ4363 Å lines, although these are always much weaker than the near-UV C lines. This behavior is illustrated in Fig. 8. As this figure shows the O lines initially rise in strength and begin to decline after the super-Eddington phase. The rate of decline of the [O III] λ5007 line is slower than that of other lines after the first few years. As a result, this line is expected to be the strongest one about a decade after the event. Moreover,

[1] The mass fraction of H was taken to be 10^{-5} and other elements were assumed to have their Solar mass fractions.

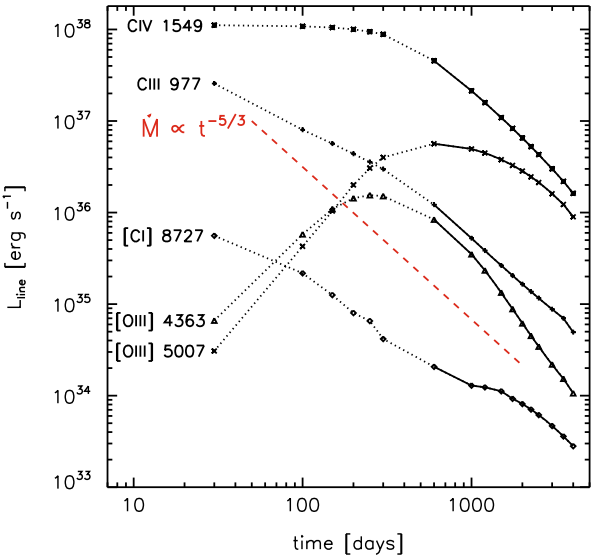

Fig. 8 Time evolution of the luminosities of the most prominent emission lines from the photoionized debris produced by the disruption of a 0.55 $M_\odot$ CO white dwarf by a 10^3 $M_\odot$ BH in a $\beta = 1$ encounter (adapted from Clausen and Eracleous 2011, see Sect. 4 of the text for the details of the models). The curves show the evolution of the luminosity of the most prominent emission lines. The dotted portion of each curve (up to 600 days) shows the evolution during and immediately after the super-Eddington accretion phase (440 days for this model), where the model predictions were deemed uncertain. The red, dashed line shows the assumed evolution of the accretion rate which sets the evolution of the strength of the ionizing continuum

since the continuum declines quickly, the observed equivalent width of the line increases in the period from a few years to a decade after the event. Clausen and Eracleous (2011) also computed the profile of the [O III] λ5007 Å line and its evolution and they found that, depending on the orientation of the observer relative to the debris tail, the profile is likely to be broad, skewed, and shifted (the shift and width can easily reach thousands of km s^{-1}).

A related family of models by Clausen et al. (2012) examines the emission lines from the debris released in the disruption of the core of an evolved star, specifically a horizontal branch star. After evolving for ∼ 10 Gyr, the core of a horizontal branch star that started out at 1 $M_\odot$, has an enhanced N abundance and suppressed C and O abundances as a result of CNO burning. Because of these modified core abundances and the depletion of hydrogen, the photoionizaiton of the debris leads to strong collisionally-excited emission lines from metals. Specifically, the [O III] λ5007 and [N II] λ6583 lines from the debris outshine the Balmer lines about a decade after the tidal disruption.

MacLeod et al. (2016b) performed radiative transfer calculations of the tidal compression of a white dwarf during a TDE to obtain predictions of their spectral and light curve properties using the hydrodynamic simulations of Rosswog et al. (2009) as input. Similarly to Type Ia supernovae, the resulting optical transients are powered by the radioactive decay of ^{56}Ni produced in the TDE. As discussed in Sect. 3, the yield of Fe-group elements will depend on the conditions of the system at the time of disruption, such as the initial white dwarf mass and composition and the β parameter. MacLeod et al. (2016b) found that the observed properties (luminosity, optical light curve decline rates, optical spectral features) of the TDEs are highly dependent on the viewing angle but in some cases have properties that are not dissimilar to unusual Type Ia supernovae but are generally less luminous (see

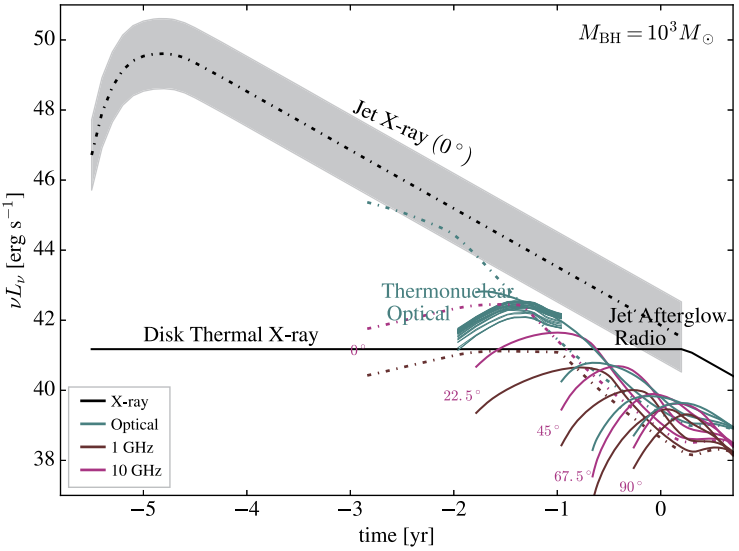

Fig. 9 The postulated multi-band signatures of a deep-passing white dwarf TDE involving a 10^3 $M_\odot$ BH and a 0.6 $M_\odot$ white dwarf. Times are from time of periapse passage of the white dwarf past the BH. This figure assumes that a jet is launched carrying kinetic energy of 6×10^{-3} times the accreted rest energy of 0.2 $M_\odot$ or 2×10^{51} erg. Line styles indicate viewing angle with respect to the jet axis: dot-dashed lines are along the jet axis, while solid lines denote an off-axis observer. Colors show different wavelengths of emission from X-ray to 1 GHz radio. At X-ray and radio wavelengths, the primary signatures are those of the jet and accretion disk. At optical wavelengths, potential signatures include the explosive transient from the thermonuclear burning of the white dwarf, depending on viewing angle, and a possible optical afterglow from the jet. For off-axis events, detection of the thermonuclear transient in the optical is a possible strategy, with accompanying X-ray emission from the accretion disk along with a radio afterglow completing the multi-wavelength picture. Adapted from MacLeod et al. (2016b, 2017)

examples in Fig. 9). This thermonuclear transient would dominate over the emission lines, such as the [O III] λλ4959,5007 and [O III] λ4363, produced by the photoionized debris tail discussed above while the transient is at its brightest but at later times these emission lines could become visible (MacLeod et al. 2016b).

5 Observational Searches and Candidates

Observational searches for the tidal disruptions of white dwarfs by IMBHs have generally taken two paths, studies looking for fast X-ray transients and optical searches for Type Ia supernova-like events. In this section we will discuss the properties of observed white dwarf TDE candidates and the link to the theoretical predictions.

5.1 Fast X-Ray Candidates

One part of the TDE transient parameter space that is still relatively unexplored is that of fast transients occurring on timescales of minutes or less. At X-ray wavelengths several events with rise times of tens of seconds have recently been discovered. Causality arguments necessitate bright transients on these timescales to be associated with compact sources, and/or

jet phenomena. The relatively low BH mass involved in a tidal disruption of a white dwarf and the compactness of the white dwarf lead to short orbital time scales. Furthermore, as the white dwarf disruption must occur in a strong gravitational field, the circularisation process is probably also short (see the contribution to this Volume by Bonnerot et al.) and as the temperature of an ensuing accretion disc scales as $T \propto M_{BH}^{-0.25}$ (assuming Eddington-limited accretion) the relatively light BHs necessarily involved in white dwarf TDEs could lead to temperatures high enough for black-body radiation to peak in soft X-rays. Alternatively, given that coronal electron populations responsible for upscattering seed photons to produce hard power-law spectra are thought to be accelerated in magnetic reconnection events (Merloni and Fabian 2001), the disruption of magnetic white dwarfs also allows for hard power-law spectra. For all these reasons, white dwarf TDEs provide appealing explanations to fast X-ray transients.

In the contribution to this Volume from Saxton et al. the properties of several of the fast X-ray transients discovered are discussed. We here present a brief recap of the properties of these transients investigating if (some of) these are viable white dwarf TDE candidates such as suggested by Jonker et al. (2013) and Shen Fast (2019), for example.

The light curve properties of the observed fast X-ray events are not uniform. The rise and decay times, observed fluxes and fluences show significant diversity. For example, the main peak(s) of the flares varied in duration between ∼50–700 seconds. Furthermore, for one event (XRT 000519; Jonker et al. 2013) two precursor flares were found, each 4000 s before the previous flare. The main peak of the flare was also split in two parts with significant spectral softening between the two peaks. Such precursor events were not detected in any of the other candidates but this may be explained by differences in orbital parameters of the disrupted white dwarfs (e.g. stars on eccentric orbits providing TDEs with precursor events and single-passage stars on parabolic orbits providing one-off flares; MacLeod et al. 2014). The timescale of the precursor flares is in line with the expected orbital timescale of a white dwarf in (an eccentric) orbit around an IMBH (cf. Fig. 5 in MacLeod et al. 2016a). Unfortunately, the distances to the sources responsible for these fast X-ray flares are in most cases not well constrained as no redshift information is available. However, for two flare events, there was spatial coincidence with Virgo cluster galaxies, making it probable that these flares occurred in the outskirts of these systems (Jonker et al. 2013; Irwin et al. 2016). The luminosities calculated assuming galaxy associations are consistent with the Eddington limit for IMBHs.

The X-ray spectral shape of these fast events is consistent with a power law (see the discussion and references in the contribution of Saxton et al. to this Volume). This is in contrast to the early-time soft X-ray spectra typically found in TDEs involving more massive black holes and stars other than white dwarfs (for some references and a discussion on differences between early- and late-time X-ray spectra of TDEs see for instance Jonker et al. 2019). It seems unlikely that a difference in the (Eddington ratio) mass accretion rate in white dwarf and main-sequence TDEs is the main cause of the different spectral shape.[2] A probable difference between main-sequence and white dwarf TDEs is the magnetic field of the star before disruption. The typically weak magnetic fields of main sequence stars may imply that their TDE discs start off with low levels of magnetic fields, whereas several white dwarf types host significant magnetic fields implying that accretion flows from white dwarf TDEs may start off with a higher magnetic field. Since power-law X-ray spectra are thought to

[2] Although the process of circularisation of the gas stream in white dwarf disruptions is affected by General Relativistic effects in contrast to many main sequence TDEs; see the contribution from Bonnerot et al. in this Volume on the formation of the accretion flow after disruption.

be caused by Compton up-scattering of seed disc photons by a coronal electron population, which in turn is thought to be accelerated to relativistic energies in magnetic reconnection events (Merloni and Fabian 2001), a power-law spectrum may more naturally emerge in the TDE discs with large magnetisation such as those occurring in white dwarf disruptions. Note that a main-sequence/longer duration TDEs with hard power law like spectra are also more difficult to distinguish from AGN activity and therefore observers may be biased against classifying such events as TDEs (Jonker et al. 2019).

The extreme source Swift J164449.3+573451 has been studied in detail, warranting a separate paragraph: it was discovered at the centre of a compact galaxy at $z = 0.35$ (Levan et al. 2011) due to its γ-ray emission. It displayed γ-ray emission lasting a few days (much longer than the duration of seconds to minutes for typical gamma-ray bursts, GRBs), as well as an extremely long-lived X-ray component. A number of models have been suggested to explain this event including a relativistic jet launched due to a TDE (Bloom et al. 2011) and the formation of an accretion disk after the collapse of a massive star to a BH (Quataert and Kasen 2012; Woosley and Heger 2012). Krolik and Piran (2011) suggested that jets from the tidal disruption of a white dwarf by an IMBH can explain the nature of this transient, in particular the short-term variability in and the fast rise time of its X-ray light curve. However, even though Tchekhovskoy et al. (2014) do not rule out that this event was powered by the tidal disruption of a white dwarf, this scenario is disfavoured according to their modelling.

There is some overlap in the X-ray properties of classical GRBs and the X-ray transients described above. Some X-ray transients have been interpreted as being caused by a GRB observed off-axis (e.g. Urata et al. 2015), as well as stripped envelope supernovae (Soderberg et al. 2005). Conversely, several ultra-long GRBs have been suggested to be associated with white dwarf TDEs (e.g. Levan et al. 2014), although other explanations have been proposed as well (e.g. Perets et al. 2016; Gao et al. 2010). In order to check the potential association, at least statistically, we compare the observed and predicted event rates.

The rate of Type Ibc SNe (some of which are associated with GRBs) is 0.258×10^{-4} Mpc^{-3} yr^{-1} and if we include the estimate from Soderberg et al. (2004) that at most 6 per cent of Type Ibc supernovae produce a collimated jet this yields a rate of 1.55×10^{-6} Type Ibc supernovae with collimated (GRB) jets per Mpc^{-3} yr^{-1}. For an assumed typical X-ray luminosity of $L_X \sim 10^{48}$ erg s^{-1} for the X-ray flash associated with the GRB, a distance limit of nearly $\sim$10 Gpc is implied given the observed X-ray fluxes of $\sim 10^{-10}$ erg cm^{-2} s^{-1} of the fast X-ray transients. Using this we derive that the Type Ibc SNe/GRB rate in this volume will be $\sim 1.5 \times 10^6$ yr^{-1}. So, comparing the observed X-ray flash rate of 1.4×10^5 yr^{-1} over the whole sky as calculated by Glennie et al. (2015) with these predicted rates, we conclude that the X-ray flashes discussed in the contribution of Saxton et al. to this Volume could be due to GRBs associated with Type Ibc supernovae. We do note that the uncertainties in these rate calculations are still substantial for instance if only due to Poisson fluctuations given the low number of detected fast X-ray flashes.

In Sect. 6 we estimate the rate of X-ray flares expected from white dwarf TDEs. The end result of those deliberations on the rate R within the volume probed with a flux limit set to $\sim 10^{-10}$ erg cm^{-2} s^{-1} is $R = f_{occ} \times 10^4$ yr^{-1}. This value falls a factor of about $14/f_{occ}$ short of the observed rate of X-ray flashes of 1.4×10^5 yr^{-1}. Of course, as indicated in Sect. 6, there are significant uncertainties in these rate calculations. Nevertheless, even optimistically assuming an occupation fraction of 1 leaves a large gap between the predictions of X-ray flares from white dwarf TDEs and the observed rate of X-ray flares. Contributions from additional populations of IMBHs, such as those that have been speculated to reside in globular clusters, or hyper–compact stellar clusters, or the lighter BHs in the recently–discovered stripped nuclei (Fragione et al. 2018; Merritt et al. 2009; Voggel et al. 2019, respectively),

may increase the rate somewhat. However, it is likely that only a small fraction of globular clusters host IMBHs and the feeding rate of white dwarfs into the loss cone is likely too low for the majority of these objects (see again also Sect. 6 for details). A high spin rate that increases the Hills mass for BHs with masses $< 10^6$ $M_\odot$ could enable IMBHs to potentially disrupt more white dwarfs but overall, it is difficult to explain all the X-ray flares as solely due to white dwarf TDEs.

5.2 Optical Candidates

As discussed in Sect. 4, if the white dwarf is tidally compressed and ignites nuclear burning then the dominant powering mechanism of optical transients in the days to weeks after disruption will be the radioactive decay of Fe-group elements, provided they are produced in sufficient amounts (e.g. in very strong encounters and/or massive white dwarfs). Each Type Ia supernova typically produces 0.6 $M_\odot$ of Fe-group elements per explosion. MacLeod et al. (2016a,b) investigated the nucleosynthetic yields of white dwarf+IMBH TDEs and found that the amount of Fe-group elements synthesised may be significantly lower than that seen in normal Type Ia supernovae, which affects their observed light curves and spectral properties.

Ca-rich transients are a class of observed optical transients with magnitudes of ~ -16 (fainter than normal Type Ia supernovae) that have strong features of Ca in their late-time spectra, suggesting that they may have appreciable Ca in their ejecta (Perets et al. 2010; Kasliwal et al. 2012; Lunnan et al. 2017). Caution in associating strong Ca features with large quantities of Ca, however, should be exercised because Ca is a very efficient coolant and a small amount of Ca in the ejecta can produce a strong feature. The early-time spectra of Ca-rich events have optical spectra that look similar to stripped envelope Type Ib SNe that typically show strong He lines (e.g. Perets et al. 2010). Various models to explain Ca-rich transients have been suggested including TDEs involving a white dwarf disrupted by an IMBH (Sell et al. 2015), a He-shell detonation on the surface of a white dwarf ('.Ia supernova' Perets et al. 2010; Shen et al. 2010), and collisions involving a He donor and a CO or ONe white dwarf (García-Berro et al. 2017). The original white dwarf TDE models are from Rosswog (2009) but radiative transfer calculations were performed by MacLeod et al. (2016b) and some low-mass white dwarf disruptions may result in transients rich in Ca. The key distinguishing characteristic for determining if Ca-rich transients are linked to TDEs involving white dwarfs and IMBHs is the detection of high-energy emission. Supernovae originating from the thermonuclear explosion of white dwarfs have not been detected in the X-ray band but X-ray emission is a key prediction of TDE models. A search for X-ray emission was made for SN 2016hnk, a white dwarf TDE candidate, but only an upper limit was placed (Sell et al. 2018) but future searches in the X-ray band will be important for testing the potential link between Ca-rich transients and white dwarf TDEs.

5.3 Multi-Wavelength Candidates

Some candidate white dwarf and IMBH TDEs have been discovered that are bright in the optical as well as having high-energy counterparts.

AT2018cow: A rapidly rising and luminous transient was discovered in the optical by Prentice et al. (2018) and also detected in the X-ray, radio, and submillimeter (Rivera Sandoval et al. 2018; Kuin et al. 2019; Margutti et al. 2018). A TDE involving a He-star and an IMBH was suggested by Ho et al. (2019). Perley et al. (2019) suggested that

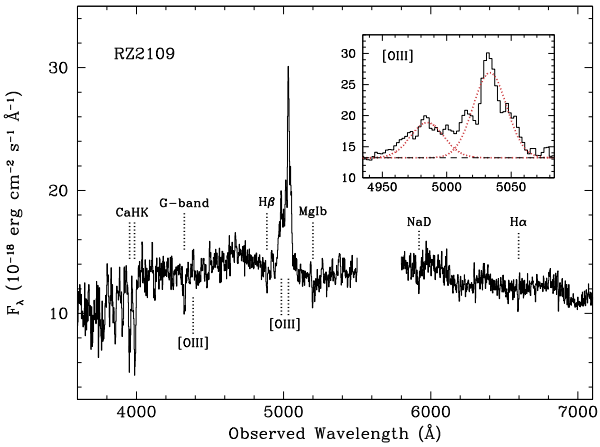

Fig. 10 The optical spectrum of the globular cluster RZ 2109 associated with the elliptical galaxy NGC 4472 in Virgo, adapted from Zepf et al. (2008). The dotted vertical lines and labels *above* the continuum identify some of the prominent absorption lines in the spectrum of an old stellar population. The dotted vertical lines and labels *below* the continuum identify three of the stronger [O III] lines expected in this range. The inset shows the profile of the [O III]4959,5007 lines with Gaussian models of FWHM $\sim 2000\,\mathrm{km\,s^{-1}}$ superposed

the transient could be caused by a main-sequence star disrupted by an IMBH but this is at odds with the detection of dense circumstellar material (detected via radio measurements) that would need to be ejected from the system prior to the TDE (Margutti et al. 2018). Other suggestions for the origin of this transient include the core-collapse of a low-mass He star or a stellar collapse involving accretion onto a newly formed compact object (Prentice et al. 2018; Margutti et al. 2018).

RZ 2109: Maccarone et al. (2007) reported the discovery of an accreting BH in the globular cluster RZ 2109, associated with the elliptical galaxy NGC 4472 in the Virgo cluster, based on its X-ray luminosity and variability properties. Followup optical spectroscopy of this object by Zepf et al. (2008) revealed the remarkable spectrum illustrated in Fig. 10, which comprises a continuum from the old stellar population of the globular cluster and a very broad emission feature identified with the [O III] λλ4959,5007 doublet (see also Steele et al. 2011). The lack of any other optical emission lines prompted Clausen and Eracleous (2011) to propose that the properties of this system were the result of the tidal disruption of a CO white dwarf by an IMBH at the centre of the cluster, accretion of some of the debris, and the photoionization of remaining, returning debris by accretion-powered ionizing radiation. This proposal was bolstered by photoionization calculations that explained the emission-line spectrum (see discussion of models in Sect. 4) and a model for the profile of the [O III] λλ5007 line that reproduced the observed profile.

However, alternative explanations were also proposed, including accretion of hydrogen-deficient material from a red giant by the BH (Porter 2010), emission from the wind of an R Corona Borealis star (Maccarone and Warner 2011), and the ionization of the ejecta of a nearby nova by the accreting BH (Ripamonti and Mapelli 2012). Moreover, some of the observed properties of RZ 2109 cannot be explained by the TDE scenario, e.g., the fact that the X-ray luminosity has remained relatively steady for about 16 years (Dage et al. 2018) and the fact that the source of the emission lines is likely to be extended (Peacock et al. 2012). Thus, the nature of the X-ray and emission-line sources

in RZ 2109 remains ambiguous. Another globular cluster with properties reminiscent of RZ 2109 was found in the elliptical galaxy NGC 1399 by Irwin et al. (2010, it is associated with the X-ray source CXO J033831.8−352604). The optical spectrum of this object features the [O III] λλ4959,5007 doublet as well as the [N II] λλ6548,6584 doublet but no other strong emission lines, which inspired Clausen et al. (2012) to explain it by invoking the disruption of a blue horizontal branch star. But all the alternative models proposed for RZ 2109 apply to this object as well.

6 Rates: Intrinsic and Predicted in Surveys

White dwarf TDEs, and their associated flares, are likely rare compared to TDEs of main sequence stars. There are several reasons for this. First, the compactness of white dwarfs implies that a more extreme tidal force is needed to disrupt them than is needed for a main sequence star. This implies a closer periapse approach to the BH is needed, and there is a correspondingly smaller cross section for these interactions. Further, only IMBHs with mass $M_\bullet \lesssim 10^5$ $M_\odot$, can accomodate these close periapse approaches without swallowing the white dwarf whole. Second, white dwarfs, while not rare in an old stellar population, are less common than low-mass main sequence stars. Nonetheless, the potentially luminous and distinct signatures of white dwarf disruption may separate these events from the larger number of main-sequence disruptions.

6.1 White Dwarf Tidal Disruption Sites and Dynamics

Just like stars of other stellar-evolutionary states, white dwarfs are tidally disrupted after passing at very close periapse distance to a massive BH. These events rely on the coexistence of massive BHs and surrounding dense clusters of stars. While highly uncertain at the BH masses most relevant to white dwarf tidal disruptions, in more massive BHs, these clusters are thought to contain roughly a BH mass of stars in a roughly isotropic, dynamically relaxed cluster surrounding the BH. Within this cluster, stars trace wandering orbits directed by both the gravitational attraction of the BH and interaction with all of the other stars. These wandering orbits occasionally are scattered to very high eccentricity, which causes them to plunge to close approaches to the BH (see the contribution of Stone et al. to this Volume on the processes that send stars on orbits that will lead to their tidal disruption).

Currently, predictions for the occurrence of white dwarf tidal disruptions come from two distinct methods: scaled-down models of stellar cusps present around more massive BHs, and N-body models of globular clusters containing IMBHs of hundreds to thousands of solar masses. We begin by examining the qualitative predictions of the nuclear cluster models. These models are discussed in detail by Merritt (2013, Chap. 6) and in the contribution of Stone et al. to this volume; they are applied to the white dwarf tidal disruption context by MacLeod et al. (2014, 2016b). In such clusters, a region of similar size to the BH sphere of gravitational influence $r_\mathrm{h} = GM_\bullet/\sigma^2$, where σ is the velocity dispersion of the surrounding stellar distribution, is assumed to contain approximately a BH mass of stars, arranged with a power-law profile in number density as a function of radius (Bahcall and Wolf 1976, 1977; Frank and Rees 1976). In the discussion that follows, we make the simplifying assumption that all stellar subtypes are distributed homogeneously within this power law profile. However, there are several reasons that this simplification may not occur in reality. Over a cluster relaxation time, stars of different mass segregate such that more massive objects end up more tightly bound to the BH than less tightly bound objects (See Chap. 7 of Merritt 2013).

This effect can be particularly strong if there is a significant population of stellar mass BHs, with mass much greater than the average cluster star (Alexander and Hopman 2009; Aharon and Perets 2016).

In scaling the properties of these clusters down from those of more massive BHs, MacLeod et al. (2014) applied the BH mass-velocity dispersion relation of Kormendy and Ho (2013), we note here that this has the consequence of determining the, a priori uncertain, density of the cluster that surrounds the putative BH. This point of uncertainty merits some caution, because, as we describe below, typical stellar densities in globular clusters (which could potentially harbor black holes of less than approximately $10^3 M_\odot$) have sufficiently low binding energy that the presence of a black hole modifies the entire cluster distribution, not just a central cusp.

With stellar cluster properties defined, one can compute the various "relaxation" properties that cause stellar orbits to change over time. In general, these include the stochastic scatterings of two-body gravitational encounters (two-body relaxation), and the coherent, secular torques applied to closer-in stellar orbits over many orbital cycles (resonant relaxation; see Merritt 2013). The typical magnitude of the per orbit random-walk in angular momentum space can be expressed in terms of the relevant relaxation timescale, $t_{\rm rel}$ as $\Delta J \approx J_{\rm c}\,(P/t_{\rm rel})^{1/2}$, where P is the orbital period and $J_{\rm c} \approx \sqrt{G M_{\rm bh} a}$ is the angular momentum of a circular orbit. This expression implies that over one relaxation time the orbital angular momentum changes by of order the circular angular momentum. Figure 11 shows the characteristic radii in such a nuclear star cluster as a function of BH mass, adapted from MacLeod et al. (2014). The line $\Delta J = J_{\rm lc}(WD)$ marks the orbital semi-major axis within the cluster where the root mean square change in orbital angular momentum over one orbit, ΔJ, equals the angular momentum of a "loss cone" orbit, $J_{\rm lc}(WD)$, that has a periapse distance similar to the white dwarf tidal radius.

At radii larger than this line, the low angular momentum phase space depleted by white dwarf tidal disruptions is repopulated each orbital period (and as a result, tidal encounters of all impact parameters occur). This is the "full loss cone" portion of the cluster phase space. At radii smaller than the $\Delta J = J_{\rm lc}(WD)$ line, the per orbit scatter is smaller than the loss cone angular momentum. This implies that the loss cone phase space is "empty" and that only grazing impact parameter encounters occur. MacLeod et al. (2014, Sect. 3) showed that most white dwarf TDEs are fed from regions where the loss cone is efficiently refilled by either two-body relaxation or mass-precession resonant relaxation. Under the assumptions of this representative cluster model, white dwarf tidal disruptions therefore occur primarily in the full loss cone limit, and therefore distribute across all periapse impact parameters.

The overall rate of white dwarf TDEs in such a model was found to be approximately 10^{-6} yr^{-1} per BH. For comparison main-sequence star TDEs occurred with a frequency of 10^{-4} yr^{-1} per BH in these same models. The white dwarf tidal disruption rate was therefore 1% of the overall tidal disruption occurrence rate. Although many assumptions must be made about the properties of stellar clusters surrounding BHs to estimate this rate, MacLeod et al. (2014, 2016b) have argued that the ratio of white dwarf to main sequence tidal disruptions may be robust with respect to variations in the system properties. Within a model in which stars are distributed in a homogenous, power-law profile, the unknown parameter with the strongest effect on the relative rates of main sequence versus white dwarf disruption events is the slope of stellar number density with radius in the central stellar cusp, which can affect relative rates at the factor ~ 2 level. A factor that could modify this conclusion is the differential mass segregation of stellar sub-populations. In essentially creating differently-sloped radial profiles of different stars (for example white dwarfs versus main-sequence stars) mass segregation might affect relative disruption rates. Perhaps more significantly, if

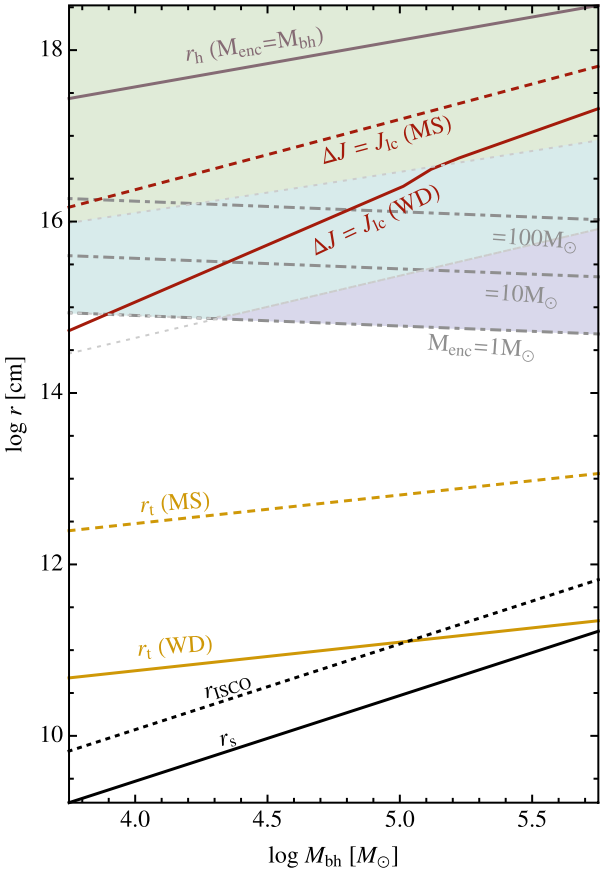

Fig. 11 Characteristic scales for interactions of white dwarfs within a central stellar cluster with the central massive BH, as a function of varying BH mass. Here the cluster is assumed to contain one BH mass of stars within the BH's sphere of gravitational influence, arranged as $n(r) \propto r^{-1.5}$. Shown, from bottom to top, are: 1) the Schwarzschild radius, r_s, and the radius of the Innermost Stable Circular Orbit $\sim 4r_s$ (black solid and dotted, respectively), 2) the tidal radius, r_t for white dwarfs ($0.5M_\odot$) and MS (sun-like) stars (yellow solid and dashed), 3) the radii that enclose 1, 10, and 100 $M_\odot$ (gray dot-dashed), 4) the characteristic orbital semi-major axis that marks the transition from the empty (smaller a) to the full (larger a) loss cone regimes (red solid and dashed lines labeled $\Delta J = J_{lc}$), and 5) the MBH radius of influence, r_h. Filled regions are, on average, populated with stars. Filling colors denote the primary orbital relaxation mechanism with general-relativistic resonant relaxation (purple), mass-precession resonant relaxation (cyan), and finally non-resonant relaxation (green) being dominant from small to large radii, respectively. Figure adapted from MacLeod et al. (2014)

a substantial population of stellar-mass BHs exists in the cluster, these could possibly or entirely occupy a portion of the tightly-bound phase space from which white dwarf disruptions are thought to arise (see, for example, the analysis of Aharon and Perets 2016, who study the related occurrence of extreme-mass ratio gravitational wave inspirals). More detailed work is needed to make quantitative statements in the context of white dwarf tidal disruptions.

The event rate of tidal disruptions by globular cluster IMBHs is thought to be considerably lower than that of galactic nuclei, on the order of 10^{-7} yr^{-1} (Ramirez-Ruiz and Rosswog 2009). In this context, N-body stellar dynamics has been the primary tool for analyzing

disruption rates. We briefly review these results, with a particular focus on the ways in which they differ from the nuclear-cluster models above.

The fundamental reasons for the use of N-body dynamics simulations in the globular cluster regime is closely related to the order of magnitude lower disruption rate predicted. The IMBH and its closely bound companion objects have a binding energy comparable to the entire cluster system. Scattering encounters act to keep the cluster core inflated to higher velocity dispersion and lower density (e.g. Baumgardt et al. 2004; MacLeod et al. 2016b). As a result of this feedback process, the presumption of an homogeneous stellar surrounding, with fixed velocity dispersion σ, is typically not realized. A related aspect of cluster–IMBH dynamics is that the IMBH wanders relative to the cluster center of mass (for general discussion and a recent analysis based on N-body simulations see, respectively, Merritt 2013; de Vita et al. 2018). A priori, this is not thought to significantly impact white dwarf disruption dynamics, because disrupted white dwarfs tend to arise from orbits that are tightly bound to the IMBH and wander relative to the cluster center with the black hole (MacLeod et al. 2016b). However, more systematic investigation may be warranted, especially if black hole masses as low as $10^3 M_\odot$ are considered. Despite these numerous differences due to overall mass scale between nuclear cluster and globular cluster dynamics we again expect of the order of 1% of the disruptions that occur will be white dwarf disruptions. The overall white dwarf disruption rate may, therefore, be of the order of 1 Gyr^{-1} per IMBH hosting globular cluster. This order of magnitude event rate has been derived from N-body simulations (Baumgardt et al. 2004; MacLeod et al. 2016b) and applied to white dwarf disruption scenarios (Haas et al. 2012; Shcherbakov et al. 2013; Sell et al. 2015). Mass segregation effects may have a stronger influence on relative event rates in this context, because globular cluster relaxation times are short relative to the age of the universe. To give a particular example, Baumgardt et al. (2004) find that white dwarfs make up approximately 8% of tidal disruptions, likely because massive white dwarfs segregate into preferentially close orbits to the IMBH when few other massive remants are present.

6.2 Occurrence of Different Classes of Encounters

We have, in the preceding section, outlined a variety of classes of white dwarf tidal disruption encounters. White dwarfs have a compactness that implies that gravitational radiation and tides act with similar strengths. Their susceptibility to explosive nuclear burning under degrees of compression that correspond to the BH tidal field further diversifies the potential outcomes. The relative occurrence of these events is a problem that lies at the interface of stellar dynamics and the processes of the events themselves.

Zalamea et al. (2010) first discussed the partial tidal stripping of white dwarfs over the course of a number of orbits with corresponding gravitational radiation (in the LISA frequency range). MacLeod et al. (2014) estimated the relative occurrence rate of these events compared to single-passage disruptions to be approximately 10% of white dwarf disruptions might occur through such a channel. However, the precise proportions remain uncertain (see Fig. 7 of MacLeod et al. 2014).

Deeply-plunging encounters, which can only occur for sufficiently low BH masses, $\lesssim 10^5$ $\mathrm{M}_\odot$, occur when the impact parameter is of the order of $\beta_{\mathrm{thermo}} \gtrsim 3$ (e.g. Rosswog et al. 2009; Anninos et al. 2018). By comparison, white dwarfs begin to lose mass at an impact parameter of $\beta_{\mathrm{ml}} \approx 0.5$. The fact that, for most parameters, the phase space of the white dwarf loss cone is thought to be efficiently refilled implies a distribution of impact parameters $N(>\beta) \propto \beta^{-1}$. In this limit, the fraction of disruptive events that pass deeply enough to lead to a thermonuclear explosion is $\beta_{\mathrm{ml}}/\beta_{\mathrm{thermo}} \sim 1/6$.

6.3 Volumetric Event Rates

The volumetric rate of white dwarf TDEs is very uncertain – mostly because the volumetric density of massive BHs below 10^6 $M_\odot$ is highly uncertain. Converting the specific rate per black-hole cluster system to a volumetric rate involves estimating the volume density of potential black-hole hosts and the BH occupation fraction in those hosts. Explicitly, $\dot{N}_{\rm vol} \approx \dot{N}_{\rm BH} n_{\rm BH}$, where $\dot{N}_{\rm BH}$ is the white dwarf TDE rate per BH (in a given mass range) and $n_{\rm BH} = n_{\rm host}\, f_{\rm BH}$ is the space density of those BHs, which is the product of the density of the hosts and the BH occupation probability for that host type. In view of the importance of the density of massive BHs, we begin the discussion of volumetric event rates by summarizing estimates of the density of potential hosts, namely dwarf galaxies and globular clusters.

An initial, theoretical estimate of $n_{\rm BH}$ can be made by a flat extrapolation of the massive BH mass function (following MacLeod et al. 2016b). Based on the results of the Illustris simulation at 10^6 $M_\odot$ (see Sijacki et al. 2015) one may infer that $n_{\rm BH} \sim 10^7$ Gpc^{-3}. Assuming a per BH rate of $\dot{N}_{\rm BH} = 10^{-6}$ yr^{-1} (see Sect. 6.1), the implied volumetric event rate is, therefore, $\dot{N}_{\rm vol} \approx 10$ yr^{-1} Gpc^{-3}. By comparison, empirical estimates based on the luminosity function or mass function of galaxies give a considerably higher density, if one assumes a high occupation fraction.

The luminosity function of galaxies can be described over the full mass range by a double Schechter function (e.g., equation (6) of Baldry et al. 2012):

$$\Phi(m)\, dm = \left[\phi_1 \left(\frac{m}{m_*} \right)^{\alpha_1} + \phi_2 \left(\frac{m}{m_*} \right)^{\alpha_2} \right] e^{-m/m_*} \frac{dm}{m_*}. \tag{19}$$

In the mass range of dwarf galaxies the exponential is approximately unity and equation (19) can be approximated as the sum of two power laws. For the purposes of our discussion, we adopt the parameters of this function reported by Wright et al. (2017), namely $\log(m_*/M_\odot) = 10.78$, $(\alpha_1, \alpha_2) = (-0.62, -1.50)$, $(\phi_1, \phi_2) = (2.93, 0.63) \times 10^{-3}$ Mpc^{-3} (assuming a Hubble constant of $H_0 = 70$ km s^{-1} Mpc^{-1}). The density of dwarf galaxies can then be found by integrating the above function. To determine suitable limits for the integration we turn to Reines et al. (2013) who studied nuclear activity in dwarf galaxies with $\log(m/M_\odot) = 8.5$–9.5 and estimated BH masses in the range $\log(M_\bullet/M_\odot) = 4.9$–$6.5$ based on the widths of the broad emission lines. Thus we integrate between $\sim 10^7$ and $10^{9.5}$ $M_\odot$ in order to include BH masses between $\sim 10^4$ and $10^{6.5}$ $M_\odot$ and we obtain a dwarf galaxy density of $n_{\rm dwarf} \approx 9 \times 10^7$ Gpc^{-3}. An alternative approach is to integrate the luminosity function of Blanton et al. (2005, expressed in terms of absolute magnitudes in their equation 8). Carrying out the integration between absolute r magnitudes of -13 and -18 using the values of the free parameters for the "total" r-band luminosity function in Table 3 of Blanton et al. (2005), adjusted to $H_0 = 70$ km s^{-1} Mpc^{-1}, we get a dwarf galaxy density of the same order as above, $n_{\rm dwarf} \approx 3 \times 10^8$ Gpc^{-3}.

The occupation fraction of BHs in these systems is unknown, although some observational constraints have been obtained. Searches for AGNs via spectroscopy or variability yield a lower limit of $f_{\rm BH} >$ a few % (Reines et al. 2013; Moran et al. 2014; Baldassare et al. 2018) while a statistical study of the X-ray properties of nearby, low-mass galaxies yields $f_{\rm BH} > 20\%$ (Miller et al. 2015). The resulting volumetric rate, based on the latter, higher dwarf galaxy density and assuming a per BH rate of $\dot{N}_{\rm BH} = 10^{-6}$ yr^{-1} (see Sect. 6.1) can be expressed as $\dot{N}_{\rm vol} \approx 300\, f_{\rm BH}$ yr^{-1} Gpc^{-3} (or $\dot{N}_{\rm vol} \gtrsim$ a few $\times$ 10 yr^{-1} Gpc^{-3}, in view of the limits on $f_{\rm BH}$).

The volume density of globular clusters can be estimated with an analogous approach. A number of recent studies (e.g., Harris et al. 2013, 2014; Zaritsky et al. 2015) show that the

number of globular clusters per massive galaxy ($m > 10^{10}$ M$_\odot$) can be expressed in terms of the mass of their host galaxy as $N_{\rm glob}(m) = N_0\,(m/m_0)^\delta$. Combining this relation with the mass function of galaxies in equation (19) we get the following density of globular clusters per unit *host galaxy* mass

$$\Phi_{\rm glob}(m)\,dm = N_0 \left(\frac{m_*}{m_0}\right)^\delta \left[\phi_1 \left(\frac{m}{m_*}\right)^{\alpha_1+\delta} + \phi_2 \left(\frac{m}{m_*}\right)^{\alpha_2+\delta}\right] e^{-m/m_*}\,\frac{dm}{m_*}. \tag{20}$$

Adopting $\log N_0 = 2.924$, $\log(m_0/{\rm M}_\odot) = 11.2$ and $\delta \approx 1$ (Harris et al. 2013), and other parameters as in equation (19) and integrating[3] for galaxy masses $m > 10^{10}$ M$_\odot$ we obtain a globular cluster volume density of $n_{\rm glob}(m > 10^{10}\ {\rm M}_\odot) = 9.5 \times 10^8\ {\rm Gpc}^{-3}$. An additional contribution may come from globular clusters associated with lower-mass galaxies. In this lower-mass range, $m = 10^8$–10^{10} M$_\odot$, the number of globular clusters per galaxy is described by a flatter power law with an index $\delta = 0.365$ and $\log N_0 = 1.274$, $\log(m_0/{\rm M}_\odot) = 9.2$ (Harris et al. 2013). Moreover, equation (20) can be simplified by neglecting the exponential, which is approximately unity for $m < 10^{10}$ M$_\odot$. Integrating $\Phi_{\rm glob}(m)$ from equation (20) in this range of galaxy masses leads to a density of $n_{\rm glob}(m = 10^8$–$10^{10}\ {\rm M}_\odot) = 4.4 \times 10^9\ {\rm Gpc}^{-3}$. But it should be borne in mind that the contribution from lower-mass galaxies is rather uncertain because the small number of globular clusters per low-mass galaxy leads to uncertain parameters for $N_{\rm glob}(m)$ in this mass range.

Searches for IMBHs have put constraints on the BH occupation fraction in globular clusters. These studies can involve measuring the dynamical properties of stars orbiting a putative IMBH in a globular cluster (e.g., Newell et al. 1976; Baumgardt et al. 2003; Gebhardt et al. 2005; Kızıltan et al. 2017; Perera et al. 2017) or measuring accretion signatures from TDEs in globular clusters, such as the IMBH candidate ESO 243-49 HLX-1 or other, similar objects (e.g., Maccarone et al. 2007; Webb et al. 2012; Lin et al. 2018). Other studies have found no signatures of accretion in large samples, suggesting that the typical masses of IMBHs in globular clusters may be lower than theoretical predictions or the occupation fraciton may be extremely small (e.g. Strader et al. 2012; Tremou et al. 2018). Using a per BH rate of $\dot{N}_{\rm BH} = 10^{-9}\ {\rm yr}^{-1}$ (see Sect. 6.1) we can express the volumetric rate as $\dot{N}_{\rm vol} \approx 4\,f_{\rm BH}\ {\rm yr}^{-1}\,{\rm Gpc}^{-3}$ or $0.2\,f_{\rm BH}\ {\rm yr}^{-1}\,{\rm Gpc}^{-3}$ depending on whether or not we include globular clusters associated with dwarf galaxies.

As the above discussion and estimates suggest, the current balance of evidence favors the cores of low-mass galaxies as the most prevalent hosts of white dwarf tidal disruptions. It is also worth emphasizing that, since BHs in globular clusters are expected to be less massive than those in dwarf galaxies the detection volume for globular cluster events should be smaller compared to dwarf galaxies because of the lower luminosities of these events.

6.4 Predicted Detectability in Surveys

In the section, we discuss the probability of the detection of white dwarf TDEs by IMBH using current X– and γ–ray missions, as well as in the future next-generation optical transient survey, the Large Synoptic Survey Telescope (LSST).

[3] The integral of the Schechter function can be expressed in terms of incomplete Γ functions, $\Gamma(p, a) = \int_a^\infty x^{p-1} e^{-x}\,dx$.

6.4.1 Detecting Beamed Emission with X– and γ–Ray Satellites

If white dwarf TDEs launch luminous jets, these will be detectable by wide-angle monitors. For example, for a jet luminosity of 10^{48} erg s^{-1}, *Swift*'s Burst Alert Telescope (BAT) will detect the event out to redshift $z \approx 1$, or a luminosity distance of 6.5 Gpc (WMAP 9 Cosmology, MacLeod et al. 2016b). The volume enclosed by redshifts $z < 1$ is approximately 150 Gpc^3. Of the population of events in this volume (see the section above) a fraction is beamed toward our observation perspective, $f_{\rm beam}$, and the BAT detects a fraction of these $f_{\rm BAT} \sim 20\%$ because of its sky coverage. The detectable rate is then

$$\dot{N}_{\rm BAT} \approx \dot{N}_{\rm vol} V f_{\rm beam} f_{\rm BAT}, \tag{21}$$

where V is the observable volume. Due to relativistic abberation, light is emitted in a narrow beam of width $1/\Gamma^2$, where Γ is the Lorentz factor. Figure 9 assumes $\Gamma \sim 7$ implying $f_{\rm beam} \sim 1/50$. However, the Lorentz factors associated with relativistic TDEs may be of the order of 2 (Zauderer et al. 2011; Cenko et al. 2012; see the contribution of Zauderer et al. to this Volume), implying a significantly larger beaming fraction of $f_{\rm beam} \sim 0.1$. Using fiducial numbers and $f_{\rm beam} \sim 1/50$ (and therefore implicitly assuming that all white dwarf TDEs lead to a jet of 10^{48} erg s^{-1}) we find $\dot{N}_{\rm BAT} \approx 6$ yr^{-1} by extrapolation of the BH mass function or $\dot{N}_{\rm BAT} \approx 180 f_{\rm BH}$ yr^{-1} from the dwarf galaxy space density.

Similarly, sensitive X–ray satellites such as *Chandra*, XMM–*Newton*, and *Swift* might serendipitously detect the X–ray flare thought to accompany a white dwarf TDE. If we again assume that the white dwarf TDE peak X-ray luminosity $L_X \sim 10^{48}$ erg s^{-1} (see Fig. 9), then the volume probed for a conservative flux limit of 10^{-10} erg cm^{-2} s^{-1} is approximately 10^3 Gpc^3. Again using the volumetric estimates of Sect. 6.3, we estimate

$$\dot{N}_{\rm X-ray} \approx \dot{N}_{\rm vol} V f_{\rm beam} f_{\rm sky}, \tag{22}$$

where $f_{\rm sky}$ is the instantaneous sky fraction observable by the X–ray satellites. This number is of the order of 6×10^{-6} for XMM–*Newton*'s pn camera with field of view of $30' \times 30'$. The number is slightly smaller for the *Swift* XRT and the *Chandra* ACIS–I detector. This fraction also assumes nearly-continuous observing. For $f_{\rm beam} = 1/50$, the implied detection rates are $\dot{N}_{\rm X-ray} \approx 1.2 \times 10^{-3}$ yr^{-1} by extrapolation of the BH mass function or $\dot{N}_{\rm X-ray} \approx 3.6 \times 10^{-2} f_{\rm BH}$ yr^{-1} from the dwarf galaxy space density. Thus, for $f_{\rm BH} \sim 1$, we could expect of the order of one detection by XMM–*Newton*, *Chandra*, or *Swift* over their roughly 20-year missions.

6.4.2 Detecting Thermonuclear Transients with LSST

Thermonuclear transients produced by the tidal disruption of a white dwarf by IMBH are well within the reach of the planned optical survey of LSST. LSST can detect a prototypical thermonuclear transient, such as that shown in Fig. 9, to $z = 0.37$ or a volume of 13.3 Gpc^3 (MacLeod et al. 2016b). We estimate the detectable rate of white-dwarf TDE thermonuclear transients as

$$\dot{N}_{\rm LSST} \approx \dot{N}_{\rm vol} V f_{\rm thermo} f_{\rm sky}, \tag{23}$$

where, $f_{\rm sky} \sim 0.5$, and thermonuclear transients are believed to occur in roughly $f_{\rm thermo} \sim 1/6$ of white dwarf TDEs, see Sect. 6.1. The resultant rates are $\dot{N}_{\rm LSST} \approx 11$ yr^{-1} based on the extrapolation of the BH mass function, or or $\dot{N}_{\rm LSST} \approx 330 f_{\rm BH}$ yr^{-1} from the dwarf

galaxy space density. There is slight viewing angle dependence introduced to these baseline estimates by the asymmetric ejecta of the tidal thermonuclear transient. See MacLeod et al. (2016b) for a Monte Carlo calculation that shows the preference for certain viewing angles.

A much greater challenge than detection of tens to hundreds of events per year will be their classification. With LSST anticipated to find hundreds of thousands of supernovae per year, only the multi-wavelength signatures of these white dwarf disruptions make them truly distinctive. One might imagine that the coincidence of high-energy and optical emission (which occurs in a smaller subset of cases, but is more distinctive) might offer one of the only paths to firm classification.

7 Multi-Messenger Signatures

7.1 Gravitational Waves from White Dwarf Inspirals Before Disruption

Since the disruptions of white dwarfs are often relativistic (i.e., the white dwarf passes within a few Schwarzschild radii from the BH), we can expect substantial emission of gravitational waves. In general terms, the frequency of gravitational waves emitted during such an encounter is of the same order as the orbital/dynamical frequency at the tidal disruption radius. This time scale is given by equation (17) and is comparable to the dynamical time of the star. For the typical white dwarf parameters considered here, $\tau_{\rm dyn} \approx 3.5\ (M_{\rm wd}/0.6\ {\rm M}_\odot)^{-1/2}\ (R_{\rm wd}/10^9\ {\rm cm})^{3/2}$ s, implying gravitational wave frequencies on the order of $f_{\rm gw} \sim 2/\tau_{\rm dyn} \sim 0.6$ Hz. This frequency is of the same order as the range accessible by the planned LASER Interferometer Space Antenna (hereafter LISA; anticipated launch date in the mid 2030s, see Danzmann 2017).

In the more likely case of a white dwarf in an unbound, parabolic orbit a burst of gravitational waves will be emitted during the initial encounter with the BH. After the initial encounter the debris will return to pericentre one dynamical time later and accretion will begin soon thereafter, leading to an electromagnetic flare. The gravitational wave strain (effectively, the observed amplitude of the wave or pulse) was computed by Rosswog et al. (2009, see their §6 for the details of the calculation and relevant formulae and references) who found it to be on the order of $h \sim 10^{-19}$, for a 0.6 $\rm M_\odot$ white dwarf passing at the tidal disruption radius of a 10^3 $\rm M_\odot$ BH at a distance of 10 kpc. This combination of parameters is appropriate for a Milky Way globular cluster, and suggests that the burst of gravitational waves from the disruption of a white dwarf in a nearby globular cluster may be detectable. However, more distant events, outside of the local group, are probably not detectable (see discussion in Anninos et al. 2018).

In an alternative and possibly rarer scenario the white dwarf is captured in a bound, typically eccentric, orbit around a BH and then spirals in. The per BH rate of such events is 1/10 the rate of all white dwarf disruptions (see discussion in Sect. 6.3). Such events are also referred to as "extreme mass ratio inspirals" (EMRIs, BH to white dwarf mass ratio $> 10^4$) or "intermediate mass ratio inspirals" (IMRIs, BH to white dwarf mass ratio 10^2–10^4). They are interesting because the white dwarf acts as a test particle that executes a very large number of orbits in the potential of the BH, hence the gravitational wave signal allows one to "map" the space-time around the BH and determine its fundamental properties: its mass and spin (see, for example, the review by Amaro-Seoane et al. 2007).

Since the white dwarf will complete a large number of orbital cycles around the BH before it is disrupted (10^5 revolutions, or even more) the gravitational wave signal is continuous and, in fact, the amplitude of the wave increases along with its frequency, as the

white dwarf spirals in. The gravitational wave strain for an IMBH in a nearby (50–100 Mpc) dwarf galaxy is $h \sim 10^{-22}$–10^{-21}. The slow inspiral allows for a detection of the gravitational wave signal with a high signal-to-noise ratio (hereafter S/N) by accumulating a large number of orbital cycles in a long "exposure" or "integration." Sesana et al. (2008) have estimated (using the methodology described in Barack and Cutler 2004) the S/N attainable by a detector with capabilities similar to those of LISA and found that such systems may be detectable with $S/N > 30$ at a distance of 100 Mpc a few years before the disruption (with an integration time of order years). Under favourable conditions (i.e., a final orbital eccentricity of zero and an integration time of 3–5 years) detections of more distant systems, up to 450 Mpc away ($z \lesssim 0.1$), are possible, although with a lower S/N. Since the orbit is (at least initially) eccentric, the higher harmonics of the signal will be stronger than the fundamental and their detection will allow determination of the fundamental system parameters, i.e., the masses of the objects involved, the distance, and the BH spin. Knowing these parameters is extremely useful for using TDEs as tools to study BH properties (as discussed in Sect. 1).

A typical event involving the inspiral of 0.6 $M_\odot$ white dwarf into a 10^5 $M_\odot$ IMBH begins with the capture of the white dwarf in a highly eccentric, bound orbit with a pericentre distance of ~ 15 R_g ($\sim 2 \times 10^{11}$ cm), corresponding to an orbital period of 3 minutes and an initial gravitational wave frequency of $f_{gw}^{init} \approx 10$ mHz (see, for example, Sesana et al. 2008; MacLeod et al. 2014, 2016a). The orbit decays gradually via the emission of gravitational waves with a possible contribution from tidal heating and radiative cooling of the white dwarf (see MacLeod et al. 2016b). The tidal heating can be amplified by resonances (e.g., Rathore et al. 2005) and can lead to substantial brightening of the white dwarf and may trigger runaway fusion in a surface layer of hydrogen (Vick et al. 2017), possibly producing a soft X-ray flare. If emission of gravitational radiation is the dominant orbital decay mechanism, the decay time is approximately 3.4 years. During this period, the system is a steady source of gravitational waves whose frequency evolves to a maximum value of $f_{gw}^{fin} \approx 120$ mHz, as the orbital separation reaches the tidal disruption radius of $R_t \approx 3$ R_g. Just before the white dwarf is disrupted, it fills its Roche lobe and goes through a phase of (stable) mass transfer onto the BH that can last days to weeks (see Zalamea et al. 2010; Dai and Blandford 2013). The accretion of this gas by the BH can lead to a substantial luminosity, on the order of 10^{43} erg s^{-1}, presumably in the X-ray band. If the orbit is still eccentric at this stage, the mass transfer, hence the X-ray emission, will also be periodic. The above scenario leads to intriguing predictions for the observational signature of this event. The first signal to be detected is the gravitational wave signal, which allows us to infer the masses of the objects involved, although the location in the sky will be fairly uncertain. This signal will also give us early warning of the TDE. The tidal heating and brightening of the white dwarf may lead to an observable, periodic signal in the optical/UV band (this is especially likely if nuclear burning is triggered on the surface of the white dwarf). Then, a few days to weeks before the ultimate disruption, we may detect steady or periodic X-ray emission as the white dwarf loses mass via Roche lobe overflow. The combination of these observational signatures holds great diagnostic power.

7.2 Ultra-High Energy Cosmic Rays from TDE Jets and Other Outflows

The jets and other outflows produced in some TDEs are also sites of particle acceleration and have been suggested as the sources of ultra-high energy cosmic rays (UHECRs, $E \gtrsim 10^{18}$ eV) and neutrinos (see, for example Farrar and Gruzinov 2009; Farrar and Piran 2014; Wang and Liu 2016; Senno et al. 2017; Lunardini and Winter 2017). Here we focus on the special conditions available in white dwarf TDEs and how they affect the process of UHECR

production. The special feature of white dwarf TDEs is that they release debris that is rich in elements heavier than helium (hereafter, "metals"), which means that the resulting jets are made up of metals. Therefore, an appreciable number of metal nuclei can survive shocks internal and external to the jet and eventually arrive at the Earth and be detected by ground-based detectors as UHECRs. This particular feature of white dwarf TDE jets is essential in explaining the composition of UHECRs.

Three recent studies have computed the composition and energy spectrum of particles that are accelerated in white dwarf TDE jets and detected as UHECRs and neutrinos: Zhang et al. (2017), Alves Batista and Silk (2017), and Biehl et al. (2018). These authors considered the acceleration of the particles, the reactions that may destroy metal nuclei, the propagation of the particles from the source to the Earth and their detection by the IceCube and Pierre Auger observatories. The general conclusion is that the models can reproduce both the composition and energy spectrum of UHECRs (Zhang et al. 2017, note that O-Ne-Mg white dwarfs lead to better agreement). The implied TDE rates range between 0.1 $\mathrm{yr}^{-1}\,\mathrm{Gpc}^{-1}$ (Biehl et al. 2018) and 10 $\mathrm{yr}^{-1}\,\mathrm{Gpc}^{-1}$ (Alves Batista and Silk 2017) but these are inversely proportional to the baryon loading of the jets (the ratio of proton to photon luminosities) and proportional to the IMBH occupation fraction (see Sect. 6.3). In view of the uncertainties in these parameters, the rates reported in this paragraph are not incompatible with those of Sect. 6.3.

8 Conclusions

This chapter provides an overview of the tidal disruption of white dwarfs by IMBHs. While no unambiguous white dwarf TDE has yet been identified, theoretical calculations and simulations suggest that if IMBHs exist, then white dwarfs will be tidally disrupted by them if they approach close enough. The subsequent detonation of the white dwarf by tidal compression is dependent on the conditions of the system but some are expected to produce observable signatures at optical wavelengths, as well as high-energy counterparts. A number of candidate events have been suggested that match many of the predicted properties but no clear case as yet been observed. The predicted intrinsic rates of white dwarf TDEs are relatively uncertain but current and future transient surveys, such as LSST, should discover them at levels where identification is possible. This will allow the physics of these extreme systems to be studied along with the implications for populations of IMBH formation and evolution.

References

D. Aharon, H.B. Perets, The impact of mass segregation and star formation on the rates of gravitational-wave sources from extreme mass ratio inspirals. Astrophys. J. Lett. **830**(1), 1 (2016). https://doi.org/10.3847/2041-8205/830/1/L1

T. Alexander, C. Hopman, Strong mass segregation around a massive black hole. Astrophys. J. **697**(2), 1861–1869 (2009). https://doi.org/10.1088/0004-637X/697/2/1861

R. Alves Batista, J. Silk, Ultrahigh-energy cosmic rays from tidally-ignited white dwarfs. Phys. Rev. D **96**(10), 103003 (2017). https://doi.org/10.1103/PhysRevD.96.103003

P. Amaro-Seoane, J.R. Gair, M. Freitag, M.C. Miller, I. Mandel, C.J. Cutler, S. Babak, TOPICAL REVIEW: intermediate and extreme mass-ratio inspirals—astrophysics, science applications and detection using LISA. Class. Quantum Gravity **24**, 113–169 (2007). https://doi.org/10.1088/0264-9381/24/17/R01

P. Anninos, P.C. Fragile, S.S. Olivier, R. Hoffman, B. Mishra, K. Camarda, Relativistic tidal disruption and nuclear ignition of white dwarf stars by intermediate-mass black holes. Astrophys. J. **865**, 3 (2018). https://doi.org/10.3847/1538-4357/aadad9

P. Anninos, R.D. Hoffman, M. Grewal, M.J. Lavell, P.C. Fragile, Nuclear ignition of white dwarf stars by relativistic encounters with rotating intermediate mass black holes. Astrophys. J. **885**(2), 136 (2019). https://doi.org/10.3847/1538-4357/ab4ae0

S. Ayal, M. Livio, T. Piran, Tidal disruption of a solar-type star by a supermassive black hole. Astrophys. J. **545**, 772–780 (2000). https://doi.org/10.1086/317835

S. Ayal, T. Piran, R. Oechslin, M.B. Davies, S. Rosswog, Post-Newtonian smoothed particle hydrodynamics. Astrophys. J. **550**, 846–859 (2001). https://doi.org/10.1086/319769

J.N. Bahcall, R.A. Wolf, Star distribution around a massive black hole in a globular cluster. Astrophys. J. **209**, 214–232 (1976). https://doi.org/10.1086/154711

J.N. Bahcall, R.A. Wolf, The star distribution around a massive black hole in a globular cluster. II Unequal star masses. Astrophys. J. **216**, 883–907 (1977). https://doi.org/10.1086/155534

V.F. Baldassare, M. Geha, J. Greene, Identifying AGNs in low-mass galaxies via long-term optical variability. Astrophys. J. **868**, 152 (2018). https://doi.org/10.3847/1538-4357/aae6cf

I.K. Baldry, S.P. Driver, J. Loveday, E.N. Taylor, L.S. Kelvin, J. Liske, P. Norberg, A.S.G. Robotham, S. Brough, A.M. Hopkins, S.P. Bamford, J.A. Peacock, J. Bland-Hawthorn, C.J. Conselice, S.M. Croom, D.H. Jones, H.R. Parkinson, C.C. Popescu, M. Prescott, R.G. Sharp, R.J. Tuffs, Galaxy And Mass Assembly (GAMA): the galaxy stellar mass function at $z < 0.06$. Mon. Not. R. Astron. Soc. **421**, 621–634 (2012). https://doi.org/10.1111/j.1365-2966.2012.20340.x

E. Bañados, B.P. Venemans, C. Mazzucchelli, E.P. Farina, F. Walter, F. Wang, R. Decarli, D. Stern, X. Fan, F.B. Davies, J.F. Hennawi, R.A. Simcoe, M.L. Turner, H.-W. Rix, J. Yang, D.D. Kelson, G.C. Rudie, J.M. Winters, An 800-million-solar-mass black hole in a significantly neutral universe at a redshift of 7.5. Nature **553**, 473–476 (2018). https://doi.org/10.1038/nature25180

L. Barack, C. Cutler, LISA capture sources: approximate waveforms, signal-to-noise ratios, and parameter estimation accuracy. Phys. Rev. D **69**(8), 082005 (2004). https://doi.org/10.1103/PhysRevD.69.082005

H. Baumgardt, J. Makino, P. Hut, S. McMillan, S. Portegies Zwart, A dynamical model for the globular cluster G1. Astrophys. J. Lett. **589**, 25–28 (2003). https://doi.org/10.1086/375802

H. Baumgardt, J. Makino, T. Ebisuzaki, Massive black holes in star clusters. I. Equal-mass clusters. Astrophys. J. **613**, 1133–1142 (2004). https://doi.org/10.1086/423298

M.C. Begelman, E.M. Rossi, P.J. Armitage, Quasi-stars: accreting black holes inside massive envelopes. Mon. Not. R. Astron. Soc. **387**, 1649–1659 (2008). https://doi.org/10.1111/j.1365-2966.2008.13344.x

D. Biehl, D. Boncioli, C. Lunardini, W. Winter, Tidally disrupted stars as a possible origin of both cosmic rays and neutrinos at the highest energies. Sci. Rep. **8**, 10828 (2018). https://doi.org/10.1038/s41598-018-29022-4

M.R. Blanton, R.H. Lupton, D.J. Schlegel, M.A. Strauss, J. Brinkmann, M. Fukugita, J. Loveday, The properties and luminosity function of extremely low luminosity galaxies. Astrophys. J. **631**, 208–230 (2005). https://doi.org/10.1086/431416

J.S. Bloom, D. Giannios, B.D. Metzger, S.B. Cenko, D.A. Perley, N.R. Butler, N.R. Tanvir, A.J. Levan, P.T. O'Brien, L.E. Strubbe, F. De Colle, E. Ramirez-Ruiz, W.H. Lee, S. Nayakshin, E. Quataert, A.R. King, A. Cucchiara, J. Guillochon, G.C. Bower, A.S. Fruchter, A.N. Morgan, A.J. van der Horst, A possible relativistic jetted outburst from a massive black hole fed by a tidally disrupted star. Science **333**, 203 (2011). https://doi.org/10.1126/science.1207150

C. Bonnerot, E.M. Rossi, G. Lodato, D.J. Price, Disc formation from stellar tidal disruptions. ArXiv e-prints (2015). arXiv:1501.04635

M. Brassart, J.P. Luminet, Shock waves in tidally compressed stars by massive black holes. Astron. Astrophys. **481**, 259 (2008)

M. Brassart, J.-P. Luminet, Relativistic tidal compressions of a star by a massive black hole. Astron. Astrophys. **511**, 80 (2010). https://doi.org/10.1051/0004-6361/200913442

S.B. Cenko, H.A. Krimm, A. Horesh, A. Rau, D.A. Frail, J.A. Kennea, A.J. Levan, S.T. Holland, N.R. Butler, R.M. Quimby, J.S. Bloom, A.V. Filippenko, A. Gal-Yam, J. Greiner, S.R. Kulkarni, E.O. Ofek, F.E. Olivares, P. Schady, J.M. Silverman, N.R. Tanvir, D. Xu, Swift J2058.4+0516: discovery of a possible second relativistic tidal disruption flare? Astrophys. J. **753**, 77 (2012). https://doi.org/10.1088/0004-637X/753/1/77

R.M. Cheng, T. Bogdanović, Tidal disruption of a star in the Schwarzschild spacetime: relativistic effects in the return rate of debris. Phys. Rev. D **90**(6), 064020 (2014). https://doi.org/10.1103/PhysRevD.90.064020

R.M. Cheng, C.R. Evans, Relativistic effects in the tidal interaction between a white dwarf and a massive black hole in Fermi normal coordinates. Phys. Rev. D **87**(10), 104010 (2013). https://doi.org/10.1103/PhysRevD.87.104010

D. Clausen, M. Eracleous, Probing intermediate-mass black holes with optical emission lines from tidally disrupted white dwarfs. Astrophys. J. **726**(1), 34 (2011)
D. Clausen, S. Sigurdsson, M. Eracleous, J.A. Irwin, Luminous [O III] and [N II] from tidally disrupted horizontal branch stars. Mon. Not. R. Astron. Soc. **424**, 1268–1274 (2012). https://doi.org/10.1111/j.1365-2966.2012.21305.x
E.R. Coughlin, C. Nixon, Variability in tidal disruption events: gravitationally unstable streams. Astrophys. J. Lett. **808**, 11 (2015). https://doi.org/10.1088/2041-8205/808/1/L11
R. Courant, K. Friedrichs, H. Lewy, Über die partiellen Differenzengleichungen der mathematischen Physik. Math. Ann. **100**, 32–74 (1928). https://doi.org/10.1007/BF01448839
K.C. Dage, S.E. Zepf, A. Bahramian, A. Kundu, T.J. Maccarone, M.B. Peacock, X-ray variability from the ultraluminous black hole candidate X-ray binary in the globular cluster RZ 2109. Astrophys. J. **862**, 108 (2018). https://doi.org/10.3847/1538-4357/aacb2b
L. Dai, R. Blandford, Roche accretion of stars close to massive black holes. Mon. Not. R. Astron. Soc. **434**, 2948–2960 (2013). https://doi.org/10.1093/mnras/stt1209
L. Dai, J.C. McKinney, N. Roth, E. Ramirez-Ruiz, M.C. Miller, A unified model for tidal disruption events. Astrophys. J. **859**(2), 20 (2018). https://doi.org/10.3847/2041-8213/aab429
K. Danzmann, *LISA and LISA Pathfinder: Laser Interferometry in Space*. Society of Photo-Optical Instrumentation Engineers (SPIE) Conference Series, vol. 10566 (Springer, Berlin, 2017), p. 1056610. https://doi.org/10.1117/12.2308272
R. de Vita, M. Trenti, M. MacLeod, Wandering off the centre: a characterization of the random motion of intermediate-mass black holes in star clusters. Mon. Not. R. Astron. Soc. **475**(2), 1574–1586 (2018). https://doi.org/10.1093/mnras/stx3261
W.E. East, Gravitational waves from the collision of tidally disrupted stars with massive black holes. Astrophys. J. **795**, 135 (2014). https://doi.org/10.1088/0004-637X/795/2/135
C.R. Evans, C.S. Kochanek, The tidal disruption of a star by a massive black hole. Astrophys. J. Lett. **346**, 13 (1989)
C. Evans, P. Laguna, M. Eracleous, Ultra-close encounters of stars with massive black holes: tidal disruption events with prompt hyperaccretion. Astrophys. J. Lett. **805**, 19 (2015). https://doi.org/10.1088/2041-8205/805/2/L19
W. Even, J.E. Tohline, Constructing synchronously rotating double white dwarf binaries. Astrophys. J. Suppl. **184**, 248–263 (2009). https://doi.org/10.1088/0067-0049/184/2/248
X. Fan, Evolution of high-redshift quasars. New Astron. Rev. **50**, 665–671 (2006). https://doi.org/10.1016/j.newar.2006.06.077
G.R. Farrar, A. Gruzinov, Giant AGN flares and cosmic ray bursts. Astrophys. J. **693**(1), 329–332 (2009). https://doi.org/10.1088/0004-637X/693/1/329
G.R. Farrar, T. Piran, Tidal disruption jets as the source of Ultra-High Energy Cosmic Rays (2014). ArXiv e-prints
G. Fragione, N.W.C. Leigh, I. Ginsburg, B. Kocsis, Tidal disruption events and gravitational waves from intermediate-mass black holes in evolving globular clusters across space and time. Astrophys. J. **867**, 119 (2018). https://doi.org/10.3847/1538-4357/aae486
J. Frank, M.J. Rees, Effects of massive central black holes on dense stellar systems. Mon. Not. R. Astron. Soc. **176**, 633–647 (1976). https://doi.org/10.1093/mnras/176.3.633
E. Gafton, S. Rosswog, Tidal disruptions by rotating black holes: effects of spin and impact parameter. Mon. Not. R. Astron. Soc. **487**, 4790–4808 (2019)
E. Gafton, E. Tejeda, J. Guillochon, O. Korobkin, S. Rosswog, Relativistic effects on tidal disruption kicks of solitary stars. Mon. Not. R. Astron. Soc. **449**, 771–780 (2015). https://doi.org/10.1093/mnras/stv350
H. Gao, Y. Lu, S.N. Zhang, A new class of gamma-ray bursts from stellar disruptions by intermediate-mass black holes. Astrophys. J. **717**(1), 268–276 (2010). https://doi.org/10.1088/0004-637X/717/1/268
E. García-Berro, C. Badenes, G. Aznar-Siguán, P. Lorén-Aguilar, White dwarf dynamical interactions and fast optical transients. Mon. Not. R. Astron. Soc. **468**(4), 4815–4821 (2017). https://doi.org/10.1093/mnras/stx813
K. Gebhardt, R.M. Rich, L.C. Ho, An intermediate-mass black hole in the globular cluster G1: improved significance from new keck and Hubble Space Telescope observations. Astrophys. J. **634**, 1093–1102 (2005). https://doi.org/10.1086/497023
A. Glennie, P.G. Jonker, R.P. Fender, T. Nagayama, M.L. Pretorius, Two fast X-ray transients in archival Chandra data. Mon. Not. R. Astron. Soc. **450**, 3765–3770 (2015). https://doi.org/10.1093/mnras/stv801
F.G. Goicovic, V. Springel, S.T. Ohlmann, R. Pakmor, Hydrodynamical moving-mesh simulations of the tidal disruption of stars by supermassive black holes (2019). arXiv e-prints
J. Guillochon, E. Ramirez-Ruiz, Hydrodynamical simulations to determine the feeding rate of black holes by the tidal disruption of stars: the importance of the impact parameter and stellar structure. Astrophys. J. **767**, 25 (2013). https://doi.org/10.1088/0004-637X/767/1/25

J. Guillochon, E. Ramirez-Ruiz, A dark year for tidal disruption events. Astrophys. J. **809**, 166 (2015). https://doi.org/10.1088/0004-637X/809/2/166
J. Guillochon, E. Ramirez-Ruiz, S. Rosswog, D. Kasen, Three-dimensional simulations of tidally disrupted solar-type stars and the observational signatures of shock breakout. Astrophys. J. **705**, 844 (2009)
J. Guillochon, H. Manukian, E. Ramirez-Ruiz, Ps1-10jh: the disruption of a main-sequence star of near-solar composition. Astrophys. J. **783**(1), 23 (2014)
R. Haas, R.V. Shcherbakov, T. Bode, P. Laguna, Tidal disruptions of white dwarfs from ultra-close encounters with intermediate-mass spinning black holes. Astrophys. J. **749**(2), 117 (2012)
W.E. Harris, G.L.H. Harris, M. Alessi, A catalog of globular cluster systems: what determines the size of a galaxy's globular cluster population? Astrophys. J. **772**, 82 (2013). https://doi.org/10.1088/0004-637X/772/2/82
G.L.H. Harris, G.B. Poole, W.E. Harris, Globular clusters and supermassive black holes in galaxies: further analysis and a larger sample. Mon. Not. R. Astron. Soc. **438**, 2117–2130 (2014). https://doi.org/10.1093/mnras/stt2337
K. Hayasaki, N. Stone, A. Loeb, Finite, intense accretion bursts from tidal disruption of stars on bound orbits. Mon. Not. R. Astron. Soc. **434**(2), 909–924 (2013)
K. Hayasaki, N. Stone, A. Loeb, Circularization of tidally disrupted stars around spinning supermassive black holes. Mon. Not. R. Astron. Soc. **461**, 3760–3780 (2016). https://doi.org/10.1093/mnras/stw1387
W.R. Hix, A.M. Khokhlov, J.C. Wheeler, F.-K. Thielemann, The quasi-equilibrium-reduced alpha-network. Astrophys. J. **503**, 332 (1998). https://doi.org/10.1086/305968
A.Y.Q. Ho, E.S. Phinney, V. Ravi, S.R. Kulkarni, G. Petitpas, B. Emonts, V. Bhalerao, R. Blundell, S.B. Cenko, D. Dobie, R. Howie, N. Kamraj, M.M. Kasliwal, T. Murphy, D.A. Perley, T.K. Sridharan, I. Yoon, AT2018cow: a luminous millimeter transient. Astrophys. J. **871**, 73 (2019). https://doi.org/10.3847/1538-4357/aaf473
M.P. Hobson, G.P. Efstathiou, A.N. Lasenby, *General Relativity* (2006). https://doi.org/10.2277/0521829518
J.A. Irwin, T.G. Brink, J.N. Bregman, T.P. Roberts, Evidence for a stellar disruption by an intermediate-mass black hole in an extragalactic globular cluster. Astrophys. J. Lett. **712**, 1–4 (2010). https://doi.org/10.1088/2041-8205/712/1/L1
J.A. Irwin, W.P. Maksym, G.R. Sivakoff, A.J. Romanowsky, D. Lin, T. Speegle, I. Prado, D. Mildebrath, J. Strader, J. Liu, J.M. Miller, Ultraluminous X-ray bursts in two ultracompact companions to nearby elliptical galaxies. Nature **538**, 356–358 (2016). https://doi.org/10.1038/nature19822
P.G. Jonker, M. Heida, M.A.P. Torres, J.C.A. Miller-Jones, A.C. Fabian, E.M. Ratti, G. Miniutti, D.J. Walton, T.P. Roberts, The nature of the bright ULX X-2 in NGC 3921: a Chandra position and HST candidate counterpart. Astrophys. J. **758**, 28 (2012). https://doi.org/10.1088/0004-637X/758/1/28
P.G. Jonker, A. Glennie, M. Heida, T. Maccarone, S. Hodgkin, G. Nelemans, J.C.A. Miller-Jones, M.A.P. Torres, R. Fender, Discovery of a new kind of explosive X-ray transient near M86. Astrophys. J. **779**, 14 (2013). https://doi.org/10.1088/0004-637X/779/1/14
P.G. Jonker, N.C. Stone, A. Generozov, S. van Velzen, B. Metzger, Implications from Late-Time X-ray Detections of Optically Selected Tidal Disruption Events: State Changes, Unification, and Detection Rates (2019). arXiv:1906.12236
M.M. Kasliwal, S.R. Kulkarni, A. Gal-Yam, P.E. Nugent, M. Sullivan, L. Bildsten, O. Yaron, H.B. Perets, I. Arcavi, S. Ben-Ami, V.B. Bhalerao, J.S. Bloom, S.B. Cenko, A.V. Filippenko, D.A. Frail, M. Ganeshalingam, A. Horesh, D.A. Howell, N.M. Law, D.C. Leonard, W. Li, E.O. Ofek, D. Polishook, D. Poznanski, R.M. Quimby, J.M. Silverman, A. Sternberg, D. Xu, Calcium-rich gap transients in the remote outskirts of galaxies. Astrophys. J. **755**(2), 161 (2012). https://doi.org/10.1088/0004-637X/755/2/161
K. Kawana, A. Tanikawa, N. Yoshida, Tidal Disruption of a White Dwarf by a Black Hole: the Diversity of Nucleosynthesis, Explosion Energy, and the Fate of Debris Streams (2017). ArXiv e-prints
S.O. Kepler, S.J. Kleinman, A. Nitta, D. Koester, B.G. Castanheira, O. Giovannini, A.F.M. Costa, L. Althaus, White dwarf mass distribution in the SDSS. Mon. Not. R. Astron. Soc. **375**, 1315–1324 (2007). https://doi.org/10.1111/j.1365-2966.2006.11388.x
M. Kesden, Black-hole spin dependence in the light curves of tidal disruption events. Phys. Rev. D **86**(6), 064026 (2012). https://doi.org/10.1103/PhysRevD.86.064026
B. Kızıltan, H. Baumgardt, A. Loeb, An intermediate-mass black hole in the centre of the globular cluster 47 Tucanae. Nature **542**, 203–205 (2017). https://doi.org/10.1038/nature21361
S. Kobayashi, P. Laguna, E.S. Phinney, P. Mészáros, Gravitational waves and x-ray signals from stellar disruption by a massive black hole. Astrophys. J. **615**, 855 (2004)
C.S. Kochanek, The aftermath of tidal disruption: the dynamics of thin gas streams. Astrophys. J. **422**, 508 (1994). https://doi.org/10.1086/173745
J. Kormendy, L.C. Ho, Coevolution (or not) of supermassive black holes and host galaxies. Annu. Rev. Astron. Astrophys. **51**, 511–653 (2013). https://doi.org/10.1146/annurev-astro-082708-101811

J.H. Krolik, T. Piran, Swift J1644+57: a white dwarf tidally disrupted by a 10^4 $M_\odot$ black hole? Astrophys. J. **743**, 134 (2011). https://doi.org/10.1088/0004-637X/743/2/134

J.H. Krolik, T. Piran, Jets from tidal disruptions of stars by black holes. Astrophys. J. **749**(1), 92 (2012)

N.P.M. Kuin, K. Wu, S. Oates, A. Lien, S. Emery, J.A. Kennea, M. de Pasquale, Q. Han, P.J. Brown, A. Tohuvavohu, A. Breeveld, D.N. Burrows, S.B. Cenko, S. Campana, A. Levan, C. Markwardt, J.P. Osborne, M.J. Page, K.L. Page, B. Sbarufatti, M. Siegel, E. Troja, Swift spectra of AT2018cow: a white dwarf tidal disruption event? Mon. Not. R. Astron. Soc. (2019). https://doi.org/10.1093/mnras/stz053

J. Law-Smith, M. MacLeod, J. Guillochon, P. Macias, E. Ramirez-Ruiz, Low-mass white dwarfs with hydrogen envelopes as a missing link in the tidal disruption menu. Astrophys. J. **841**(2), 132 (2017). https://doi.org/10.3847/1538-4357/aa6ffb

A.J. Levan, N.R. Tanvir, S.B. Cenko, D.A. Perley, K. Wiersema, J.S. Bloom, A.S. Fruchter, A.D.U. Postigo, P.T. O'Brien, N. Butler, A.J. van der Horst, G. Leloudas, A.N. Morgan, K. Misra, G.C. Bower, J. Farihi, R.L. Tunnicliffe, M. Modjaz, J.M. Silverman, J. Hjorth, C. Thöne, A. Cucchiara, J.M.C. Cerón, A.J. Castro-Tirado, J.A. Arnold, M. Bremer, J.P. Brodie, T. Carroll, M.C. Cooper, P.A. Curran, R.M. Cutri, J. Ehle, D. Forbes, J. Fynbo, J. Gorosabel, J. Graham, D.I. Hoffman, S. Guziy, P. Jakobsson, A. Kamble, T. Kerr, M.M. Kasliwal, C. Kouveliotou, D. Kocevski, N.M. Law, P.E. Nugent, E.O. Ofek, D. Poznanski, R.M. Quimby, E. Rol, A.J. Romanowsky, R. Sánchez-Ramírez, S. Schulze, N. Singh, L. van Spaandonk, R.L.C. Starling, R.G. Strom, J.C. Tello, O. Vaduvescu, P.J. Wheatley, R.A.M.J. Wijers, J.M. Winters, D. Xu, An extremely luminous panchromatic outburst from the nucleus of a distant galaxy. Science **333**, 199 (2011). https://doi.org/10.1126/science.1207143

A.J. Levan, N.R. Tanvir, R.L.C. Starling, K. Wiersema, K.L. Page, D.A. Perley, S. Schulze, G.A. Wynn, R. Chornock, J. Hjorth, S.B. Cenko, A.S. Fruchter, P.T. O'Brien, G.C. Brown, R.L. Tunnicliffe, D. Malesani, P. Jakobsson, D. Watson, E. Berger, D. Bersier, B.E. Cobb, S. Covino, A. Cucchiara, A. de Ugarte Postigo, D.B. Fox, A. Gal-Yam, P. Goldoni, J. Gorosabel, L. Kaper, T. Krühler, R. Karjalainen, J.P. Osborne, E. Pian, R. Sánchez-Ramírez, B. Schmidt, I. Skillen, G. Tagliaferri, C. Thöne, O. Vaduvescu, R.A.M.J. Wijers, B.A. Zauderer, A new population of ultra-long duration gamma-ray bursts. Astrophys. J. **781**, 13 (2014). https://doi.org/10.1088/0004-637X/781/1/13

D. Lin, J. Strader, E.R. Carrasco, D. Page, A.J. Romanowsky, J. Homan, J.A. Irwin, R.A. Remillard, O. Godet, N.A. Webb, H. Baumgardt, R. Wijnands, D. Barret, P.-A. Duc, J.P. Brodie, S.D.J. Gwyn, A luminous X-ray outburst from an intermediate-mass black hole in an off-centre star cluster. Nat. Astron. (2018). https://doi.org/10.1038/s41550-018-0493-1

G. Lodato, E.M. Rossi, Multiband light curves of tidal disruption events. Mon. Not. R. Astron. Soc. **410**(1), 359–367 (2011). https://doi.org/10.1111/j.1365-2966.2010.17448.x

G. Lodato, A.R. King, J.E. Pringle, Stellar disruption by a supermassive black hole: is the light curve really proportional to t-5/3? Mon. Not. R. Astron. Soc. **392**, 332 (2009)

J.P. Luminet, B. Carter, Dynamics of an affine star model in a black hole tidal field. Astrophys. J. Suppl. **61**, 219 (1986)

J. Luminet, J.-A. Marck, Tidal squeezing of stars by Schwarzschild black holes. Mon. Not. R. Astron. Soc. **212**, 57 (1985)

J. Luminet, B. Pichon, Tidal pinching of white dwarfs. Astron. Astrophys. **209**, 103 (1989)

C. Lunardini, W. Winter, High energy neutrinos from the tidal disruption of stars. Phys. Rev. D **95**(12), 123001 (2017). https://doi.org/10.1103/PhysRevD.95.123001

R. Lunnan, M.M. Kasliwal, Y. Cao, L. Hangard, O. Yaron, J.T. Parrent, C. McCully, A. Gal-Yam, J.S. Mulchaey, S. Ben-Ami, A.V. Filippenko, C. Fremling, A.S. Fruchter, D.A. Howell, J. Koda, T. Kupfer, S.R. Kulkarni, R. Laher, F. Masci, P.E. Nugent, E.O. Ofek, M. Yagi, L. Yan, Two new calcium-rich gap transients in group and cluster environments. Astrophys. J. **836**(1), 60 (2017). https://doi.org/10.3847/1538-4357/836/1/60

T.J. Maccarone, B. Warner, Strong [O III] and [N II] emission lines in globular clusters from photoionized R corona borealis star winds. Mon. Not. R. Astron. Soc. **410**, 32–36 (2011). https://doi.org/10.1111/j.1745-3933.2010.00973.x

T.J. Maccarone, A. Kundu, S.E. Zepf, K.L. Rhode, A black hole in a globular cluster. Nature **445**, 183–185 (2007). https://doi.org/10.1038/nature05434

M. MacLeod, J. Goldstein, E. Ramirez-Ruiz, J. Guillochon, J. Samsing, Illuminating massive black holes with white dwarfs: orbital dynamics and high-energy transients from tidal interactions. Astrophys. J. **794**, 9 (2014). https://doi.org/10.1088/0004-637X/794/1/9

M. MacLeod, M. Trenti, E. Ramirez-Ruiz, The close stellar companions to intermediate-mass black holes. Astrophys. J. **819**, 70 (2016a). https://doi.org/10.3847/0004-637X/819/1/70

M. MacLeod, J. Guillochon, E. Ramirez-Ruiz, D. Kasen, S. Rosswog, Optical thermonuclear transients from tidal compression of white dwarfs as tracers of the low end of the massive black hole mass function. Astrophys. J. **819**, 3 (2016b). https://doi.org/10.3847/0004-637X/819/1/3

M. MacLeod, J. Guillochon, E. Ramirez-Ruiz, D. Kasen, S. Rosswog, Erratum: "Optical thermonuclear transients from tidal compression of white dwarfs as tracers of the low end of the massive black hole mass function". Astrophys. J. **843**, 154 (2017). https://doi.org/10.3847/1538-4357/aa7b74

R. Margutti, B.D. Metzger, R. Chornock, I. Vurm, N. Roth, B.W. Grefenstette, V. Savchenko, R. Cartier, J.F. Steiner, G. Terreran, G. Migliori, D. Milisavljevic, K.D. Alexander, M. Bietenholz, P.K. Blanchard, E. Bozzo, D. Brethauer, I.V. Chilingarian, D.L. Coppejans, L. Ducci, C. Ferrigno, W. Fong, D. GÖtz, C. Guidorzi, A. Hajela, K. Hurley, E. Kuulkers, P. Laurent, S. Mereghetti, M. Nicholl, D. Patnaude, P. Ubertini, J. Banovetz, N. Bartel, E. Berger, E.R. Coughlin, T. Eftekhari, D.D. Frederiks, A.V. Kozlova, T. Laskar, D.S. Svinkin, M.R. Drout, A. Macfadyen, K. Paterson, An embedded X-ray source shines through the aspherical AT2018cow: revealing the inner workings of the most luminous fast-evolving optical transients (2018). arXiv e-prints

L. Mayer, S. Kazantzidis, A. Escala, S. Callegari, Direct formation of supermassive black holes via multi-scale gas inflows in galaxy mergers. Nature **466**, 1082–1084 (2010). https://doi.org/10.1038/nature09294

N.J. McConnell, C.-P. Ma, Revisiting the scaling relations of black hole masses and host galaxy properties. Astrophys. J. **764**, 184 (2013). https://doi.org/10.1088/0004-637X/764/2/184

A. Merloni, A.C. Fabian, Accretion disc coronae as magnetic reservoirs. Mon. Not. R. Astron. Soc. **321**, 549–552 (2001). https://doi.org/10.1046/j.1365-8711.2001.04060.x

D. Merritt, *Dynamics and Evolution of Galactic Nuclei* (2013)

D. Merritt, J.D. Schnittman, S. Komossa, Hypercompact stellar systems around recoiling supermassive black holes. Astrophys. J. **699**, 1690–1710 (2009). https://doi.org/10.1088/0004-637X/699/2/1690

B.P. Miller, E. Gallo, J.E. Greene, B.C. Kelly, T. Treu, J.-H. Woo, V. Baldassare, X-ray constraints on the local supermassive black hole occupation fraction. Astrophys. J. **799**, 98 (2015). https://doi.org/10.1088/0004-637X/799/1/98

J.J. Monaghan, Smoothed particle hydrodynamics. Rep. Prog. Phys. **68**, 1703–1759 (2005). https://doi.org/10.1088/0034-4885/68/8/R01

E.C. Moran, K. Shahinyan, H.R. Sugarman, D.O. Vélez, M. Eracleous, Black holes at the centers of nearby dwarf galaxies. Astron. J. **148**, 136 (2014). https://doi.org/10.1088/0004-6256/148/6/136

D.J. Mortlock, S.J. Warren, B.P. Venemans, M. Patel, P.C. Hewett, R.G. McMahon, C. Simpson, T. Theuns, E.A. Gonzáles-Solares, A. Adamson, S. Dye, N.C. Hambly, P. Hirst, M.J. Irwin, E. Kuiper, A. Lawrence, H.J.A. Röttgering, A luminous quasar at a redshift of z = 7.085. Nature **474**, 616–619 (2011). https://doi.org/10.1038/nature10159

E. Müller, Simulation of astrophysical fluid flow, in *Computational methods for astrophysical fluid flow*, ed. by O. Steiner, A. Gautschy (Springer, Berlin, 1998)

M. Nauenberg, Analytic approximations to the mass-radius relation and energy of zero-temperature stars. Astrophys. J. **175**, 417 (1972). https://doi.org/10.1086/151568

B. Newell, G.S. Da Costa, J. Norris, Evidence for a central massive object in the X-ray cluster M15. Astrophys. J. Lett. **208**, 55 (1976). https://doi.org/10.1086/182232

M.B. Peacock, S.E. Zepf, A. Kundu, T.J. Maccarone, K.L. Rhode, J.J. Salzer, C.Z. Waters, R. Ciardullo, C. Gronwall, D. Stern, Spatially resolved spectroscopy of the globular cluster RZ 2109 and the nature of its black hole. Astrophys. J. **759**, 126 (2012). https://doi.org/10.1088/0004-637X/759/2/126

B.B.P. Perera, B.W. Stappers, A.G. Lyne, C.G. Bassa, I. Cognard, L. Guillemot, M. Kramer, G. Theureau, G. Desvignes, Evidence for an intermediate-mass black hole in the globular cluster NGC 6624. Mon. Not. R. Astron. Soc. **468**, 2114–2127 (2017). https://doi.org/10.1093/mnras/stx501

H.B. Perets, A. Gal-Yam, P.A. Mazzali, D. Arnett, D. Kagan, A.V. Filippenko, W. Li, I. Arcavi, S.B. Cenko, D.B. Fox, D.C. Leonard, D.-S. Moon, D.J. Sand, A.M. Soderberg, J.P. Anderson, P.A. James, R.J. Foley, M. Ganeshalingam, E.O. Ofek, L. Bildsten, G. Nelemans, K.J. Shen, N.N. Weinberg, B.D. Metzger, A.L. Piro, E. Quataert, M. Kiewe, D. Poznanski, A faint type of supernova from a white dwarf with a helium-rich companion. Nature **465**(7296), 322–325 (2010). https://doi.org/10.1038/nature09056

H.B. Perets, Z. Li, J.C. Lombardi Jr., S.R. Milcarek Jr., Micro-tidal disruption events by stellar compact objects and the production of ultra-long GRBs. Astrophys. J. **823**(2), 113 (2016). https://doi.org/10.3847/0004-637X/823/2/113

D.A. Perley, P.A. Mazzali, L. Yan, S.B. Cenko, S. Gezari, K. Taggart, N. Blagorodnova, C. Fremling, B. Mockler, A. Singh, N. Tominaga, M. Tanaka, A.M. Watson, T. Ahumada, G.C. Anupama, C. Ashall, R.L. Becerra, D. Bersier, V. Bhalerao, J.S. Bloom, N.R. Butler, C. Copperwheat, M.W. Coughlin, K. De, A.J. Drake, D.A. Duev, S. Frederick, J.J. González, A. Goobar, M. Heida, A.Y.Q. Ho, J. Horst, T. Hung, R. Itoh, J.E. Jencson, M.M. Kasliwal, N. Kawai, T. Khanam, S.R. Kulkarni, B. Kumar, H. Kumar, A.S. Kutyrev, W.H. Lee, K. Maeda, A. Mahabal, K.L. Murata, J.D. Neill, C.-C. Ngeow, B. Penprase, E. Pian, R. Quimby, E. Ramirez-Ruiz, M.G. Richer, C.G. Román-Zúñiga, D.K. Sahu, S. Srivastav, Q. Socia, J. Sollerman, Y. Tachibana, F. Taddia, S. Tinyanont, E. Troja, C. Ward, J. Wee, P.-C. Yu, The fast, luminous

ultraviolet transient AT2018cow: extreme supernova, or disruption of a star by an intermediate-mass black hole? Mon. Not. R. Astron. Soc. **484**, 1031–1049 (2019). https://doi.org/10.1093/mnras/sty3420
E.S. Phinney, Manifestations of a massive black hole in the galactic center, in *IAU Symp. 136: The Center of the Galaxy*, ed. by M. Morris (1989), p. 543
S.F. Portegies Zwart, S.L.W. McMillan, The runaway growth of intermediate-mass black holes in dense star clusters. Astrophys. J. **576**, 899–907 (2002). https://doi.org/10.1086/341798
R.L. Porter, Broad and luminous [OIII] and [NII] in globular cluster ULXs. Mon. Not. R. Astron. Soc. **407**, 59–63 (2010). https://doi.org/10.1111/j.1745-3933.2010.00904.x
S.J. Prentice, K. Maguire, S.J. Smartt, M.R. Magee, P. Schady, S. Sim, T.-W. Chen, P. Clark, C. Colin, M. Fulton, O. McBrien, D. O'Neill, K.W. Smith, C. Ashall, K.C. Chambers, L. Denneau, H.A. Flewelling, A. Heinze, T.W.-S. Holoien, M.E. Huber, C.S. Kochanek, P.A. Mazzali, J.L. Prieto, A. Rest, B.J. Shappee, B. Stalder, K.Z. Stanek, M.D. Stritzinger, T.A. Thompson, J.L. Tonry, The cow: discovery of a luminous, hot, and rapidly evolving transient. Astrophys. J. Lett. **865**, 3 (2018). https://doi.org/10.3847/2041-8213/aadd90
E. Quataert, D. Kasen, Swift 1644+57: the longest gamma-ray burst? Mon. Not. R. Astron. Soc. **419**, 1–5 (2012). https://doi.org/10.1111/j.1745-3933.2011.01151.x
E. Ramirez-Ruiz, S. Rosswog, The star ingesting luminosity of intermediate-mass black holes in globular clusters. Astrophys. J. Lett. **697**, 77–80 (2009). https://doi.org/10.1088/0004-637X/697/2/L77
E. Rantsiou, S. Kobayashi, P. Laguna, F.A. Rasio, Mergers of black hole-neutron star binaries. I. Methods and first results. Astrophys. J. **680**, 1326–1349 (2008). https://doi.org/10.1086/587858
Y. Rathore, R.D. Blandford, A.E. Broderick, Resonant excitation of white dwarf oscillations in compact object binaries - I. The no back reaction approximation. Mon. Not. R. Astron. Soc. **357**(3), 834–846 (2005). https://doi.org/10.1111/j.1365-2966.2004.08459.x
M.J. Rees, Tidal disruption of stars by black holes of 10 to the 6th-10 to the 8th solar masses in nearby galaxies. Nature **333**, 523 (1988)
A.E. Reines, J.E. Greene, M. Geha, Dwarf galaxies with optical signatures of active massive black holes. Astrophys. J. **775**, 116 (2013). https://doi.org/10.1088/0004-637X/775/2/116
E. Ripamonti, M. Mapelli, Broad [O III] in the globular cluster RZ 2109: X-ray ionized nova ejecta. Mon. Not. R. Astron. Soc. **423**, 1144–1153 (2012). https://doi.org/10.1111/j.1365-2966.2012.20942.x
L.E. Rivera Sandoval, T.J. Maccarone, A. Corsi, P.J. Brown, D. Pooley, J.C. Wheeler, X-ray Swift observations of SN 2018cow. Mon. Not. R. Astron. Soc. **480**, 146–150 (2018). https://doi.org/10.1093/mnrasl/sly145
S. Rosswog, Astrophysical smooth particle hydrodynamics. New Astron. Rev. **53**, 78–104 (2009). https://doi.org/10.1016/j.newar.2009.08.007
S. Rosswog, SPH methods in the modelling of compact objects. Living Rev. Comput. Astrophys. **1**, 1 (2015). https://doi.org/10.1007/lrca-2015-1
S. Rosswog, The Lagrangian hydrodynamics code MAGMA2 (2019). arXiv:1911.13093
S. Rosswog, E. Ramirez-Ruiz, W.R. Hix, Tidal disruption and ignition of white dwarfs by moderately massive black holes. Astrophys. J. **695**(1), 404–419 (2009)
N. Roth, D. Kasen, J. Guillochon, E. Ramirez-Ruiz, The X-ray through optical fluxes and line strengths of tidal disruption events. Astrophys. J. **827**, 3 (2016). https://doi.org/10.3847/0004-637X/827/1/3
A. Sądowski, E. Tejeda, E. Gafton, S. Rosswog, D. Abarca, Magnetohydrodynamical simulations of a deep tidal disruption in general relativity. Mon. Not. R. Astron. Soc. **458**, 4250–4268 (2016). https://doi.org/10.1093/mnras/stw589
P.H. Sell, T.J. Maccarone, R. Kotak, C. Knigge, D.J. Sand, Calcium-rich gap transients: tidal detonations of white dwarfs? Mon. Not. R. Astron. Soc. **450**, 4198–4206 (2015). https://doi.org/10.1093/mnras/stv902
P.H. Sell, K. Arur, T.J. Maccarone, R. Kotak, C. Knigge, D.J. Sand, S. Valenti, Chandra X-ray constraints on the candidate Ca-rich gap transient SN 2016hnk. Mon. Not. R. Astron. Soc. **475**, 111–115 (2018). https://doi.org/10.1093/mnrasl/sly011
N. Senno, K. Murase, P. Mészáros, High-energy neutrino flares from X-ray bright and dark tidal disruption events. Astrophys. J. **838**(1), 3 (2017). https://doi.org/10.3847/1538-4357/aa6344
A. Sesana, A. Vecchio, M. Eracleous, S. Sigurdsson, Observing white dwarfs orbiting massive black holes in the gravitational wave and electro-magnetic window. Mon. Not. R. Astron. Soc. **391**, 718–726 (2008). https://doi.org/10.1111/j.1365-2966.2008.13904.x
R.V. Shcherbakov, A. Pe'er, C.S. Reynolds, R. Haas, T. Bode, P. Laguna, Grb060218 as a tidal disruption of a white dwarf by an intermediate-mass black hole. Astrophys. J. **769**(2), 85 (2013)
g-F. Shen Fast, Ultraluminous X-ray bursts from tidal stripping of white dwarfs by intermediate-mass black holes. Astrophys. J. Lett. **871**, 17 (2019). https://doi.org/10.3847/2041-8213/aafc64
K.J. Shen, D. Kasen, N.N. Weinberg, L. Bildsten, E. Scannapieco, Thermonuclear Ia supernovae from helium shell detonations: explosion models and observables. Astrophys. J. **715**(2), 767–774 (2010). https://doi.org/10.1088/0004-637X/715/2/767

H. Shiokawa, J.H. Krolik, R.M. Cheng, T. Piran, S.C. Noble, General relativistic hydrodynamic simulation of accretion flow from a stellar tidal disruption. Astrophys. J. **804**, 85 (2015). https://doi.org/10.1088/0004-637X/804/2/85

D. Sijacki, M. Vogelsberger, S. Genel, V. Springel, P. Torrey, G.F. Snyder, D. Nelson, L. Hernquist, The illustris simulation: the evolving population of black holes across cosmic time. Mon. Not. R. Astron. Soc. **452**, 575–596 (2015). https://doi.org/10.1093/mnras/stv1340

J. Silk, Feedback by massive black holes in gas-rich dwarf galaxies. Astrophys. J. Lett. **839**, 13 (2017). https://doi.org/10.3847/2041-8213/aa67da

A.M. Soderberg, D.A. Frail, M.H. Wieringa, Constraints on off-axis gamma-ray burst jets in type ibc supernovae from late-time radio observations. Astrophys. J. Lett. **607**, 13–16 (2004). https://doi.org/10.1086/421722

A.M. Soderberg, S.R. Kulkarni, D.B. Fox, E. Berger, P.A. Price, S.B. Cenko, D.A. Howell, A. Gal-Yam, D.C. Leonard, D.A. Frail, D. Moon, R.A. Chevalier, M. Hamuy, K.C. Hurley, D. Kelson, K. Koviak, W. Krzeminski, P. Kumar, A. MacFadyen, P.J. McCarthy, H.S. Park, B.A. Peterson, M.M. Phillips, M. Rauch, M. Roth, B.P. Schmidt, S. Shectman, An HST search for supernovae accompanying X-ray flashes. Astrophys. J. **627**, 877–887 (2005). https://doi.org/10.1086/430405

V. Springel, Smoothed particle hydrodynamics in astrophysics. Annu. Rev. Astron. Astrophys. **48**, 391–430 (2010). https://doi.org/10.1146/annurev-astro-081309-130914

M.M. Steele, S.E. Zepf, A. Kundu, T.J. Maccarone, K.L. Rhode, J.J. Salzer, Velocity structure and variability of [O III] emission in black hole host globular cluster RZ2109. Astrophys. J. **739**, 95 (2011). https://doi.org/10.1088/0004-637X/739/2/95

N. Stone, R. Sari, A. Loeb, Consequences of strong compression in tidal disruption events. Mon. Not. R. Astron. Soc. **435**(3), 1809–1824 (2013)

J. Strader, L. Chomiuk, T.J. Maccarone, J.C.A. Miller-Jones, A.C. Seth, C.O. Heinke, G.R. Sivakoff, No evidence for intermediate-mass black holes in globular clusters: strong constraints from the JVLA. Astrophys. J. Lett. **750**, 27 (2012). https://doi.org/10.1088/2041-8205/750/2/L27

L.E. Strubbe, E. Quataert, Optical flares from the tidal disruption of stars by massive black holes. Mon. Not. R. Astron. Soc. **400**, 2070 (2009)

L.E. Strubbe, E. Quataert, Spectroscopic signatures of the tidal disruption of stars by massive black holes. Mon. Not. R. Astron. Soc. **415**(1), 168–180 (2011)

A. Tanikawa, High-resolution hydrodynamic simulation of tidal detonation of a helium white dwarf by an intermediate mass black hole. Astrophys. J. **858**(1), 26 (2018a). https://doi.org/10.3847/1538-4357/aaba79

A. Tanikawa, Tidal double detonation: a new mechanism for the thermonuclear explosion of a white dwarf induced by a tidal disruption event. Mon. Not. R. Astron. Soc. **475**(1), 67–71 (2018b). https://doi.org/10.1093/mnrasl/sly006

A. Tanikawa, Y. Sato, K. Nomoto, K. Maeda, N. Nakasato, I. Hachisu, Does explosive nuclear burning occur in tidal disruption events of white dwarfs by intermediate-mass black holes? Astrophys. J. **839**, 81 (2017). https://doi.org/10.3847/1538-4357/aa697d

A. Tchekhovskoy, B.D. Metzger, D. Giannios, L.Z. Kelley, Swift J1644+57 gone MAD: the case for dynamically important magnetic flux threading the black hole in a jetted tidal disruption event. Mon. Not. R. Astron. Soc. **437**, 2744–2760 (2014). https://doi.org/10.1093/mnras/stt2085

E. Tejeda, S. Rosswog, An accurate Newtonian description of particle motion around a Schwarzschild black hole. Mon. Not. R. Astron. Soc. **433**, 1930–1940 (2013). https://doi.org/10.1093/mnras/stt853

E. Tejeda, E. Gafton, S. Rosswog, Tidal disruptions by rotating black holes: relativistic hydrodynamics with Newtonian codes (2017). ArXiv e-prints

E. Tremou, J. Strader, L. Chomiuk, L. Shishkovsky, T.J. Maccarone, J.C.A. Miller-Jones, V. Tudor, C.O. Heinke, G.R. Sivakoff, A.C. Seth, E. Noyola, The MAVERIC survey: still no evidence for accreting intermediate-mass black holes in globular clusters. Astrophys. J. **862**, 16 (2018). https://doi.org/10.3847/1538-4357/aac9b9

Y. Urata, K. Huang, R. Yamazaki, T. Sakamoto, Extremely soft x-ray flash as the indicator of off-axis orphan GRB afterglow. Astrophys. J. **806**(2), 222 (2015). https://doi.org/10.1088/0004-637x/806/2/222

M. Vick, D. Lai, J. Fuller, Tidal dissipation and evolution of white dwarfs around massive black holes: an eccentric path to tidal disruption. Mon. Not. R. Astron. Soc. **468**, 2296–2310 (2017). https://doi.org/10.1093/mnras/stx539

K.T. Voggel, A.C. Seth, H. Baumgardt, S. Mieske, J. Pfeffer, A. Rasskazov, The impact of stripped nuclei on the supermassive black hole number density in the local universe. Astrophys. J. **871**, 159 (2019). https://doi.org/10.3847/1538-4357/aaf735

M. Volonteri, The formation and evolution of massive black holes. Science **337**, 544 (2012). https://doi.org/10.1126/science.1220843

X.-Y. Wang, R.-Y. Liu, Tidal disruption jets of supermassive black holes as hidden sources of cosmic rays: explaining the IceCube TeV-PeV neutrinos. Phys. Rev. D **93**(8), 083005 (2016). https://doi.org/10.1103/PhysRevD.93.083005

N. Webb, D. Cseh, E. Lenc, O. Godet, D. Barret, S. Corbel, S. Farrell, R. Fender, N. Gehrels, I. Heywood, Radio detections during two state transitions of the intermediate-mass black hole HLX-1. Science **337**, 554 (2012). https://doi.org/10.1126/science.1222779

S.E. Woosley, A. Heger, Long gamma-ray transients from collapsars. Astrophys. J. **752**, 32 (2012). https://doi.org/10.1088/0004-637X/752/1/32

A.H. Wright, A.S.G. Robotham, S.P. Driver, M. Alpaslan, S.K. Andrews, I.K. Baldry, J. Bland-Hawthorn, S. Brough, M.J.I. Brown, M. Colless et al., Galaxy and mass assembly (gama): the galaxy stellar mass function to z = 0.1 from the R-band selected equatorial regions. Mon. Not. R. Astron. Soc. **470**(1), 283–302 (2017). https://doi.org/10.1093/mnras/stx1149

I. Zalamea, K. Menou, A.M. Beloborodov, White dwarfs stripped by massive black holes: sources of co-incident gravitational and electromagnetic radiation. Mon. Not. R. Astron. Soc. **409**, 25–29 (2010). https://doi.org/10.1111/j.1745-3933.2010.00930.x

D. Zaritsky, M. Aravena, E. Athanassoula, A. Bosma, S. Comerón, B.G. Elmegreen, S. Erroz-Ferrer, D.A. Gadotti, J.L. Hinz, L.C. Ho et al., Globular cluster populations: first results from s4g early-type galaxies. Astrophys. J. **799**(2), 159 (2015). https://doi.org/10.1088/0004-637x/799/2/159

B.A. Zauderer, E. Berger, A.M. Soderberg, A. Loeb, R. Narayan, D.A. Frail, G.R. Petitpas, A. Brunthaler, R. Chornock, J.M. Carpenter, G.G. Pooley, K. Mooley, S.R. Kulkarni, R. Margutti, D.B. Fox, E. Nakar, N.A. Patel, N.H. Volgenau, T.L. Culverhouse, M.F. Bietenholz, M.P. Rupen, W. Max-Moerbeck, A.C.S. Readhead, J. Richards, M. Shepherd, S. Storm, C.L.H. Hull, Birth of a relativistic outflow in the unusual γ-ray transient Swift j164449.3+573451. Nature **476**(7), 425–428 (2011)

S.E. Zepf, D. Stern, T.J. Maccarone, A. Kundu, M. Kamionkowski, K.L. Rhode, J.J. Salzer, R. Ciardullo, C. Gronwall, Very broad [O III] $\lambda\lambda$4959, 5007 emission from the NGC 4472 globular cluster RZ 2109 and implications for the mass of its black hole X-ray source. Astrophys. J. Lett. **683**, 139 (2008). https://doi.org/10.1086/591937

B.T. Zhang, K. Murase, F. Oikonomou, Z. Li, High-energy cosmic ray nuclei from tidal disruption events: origin, survival, and implications. Phys. Rev. D **96**(6), 063007 (2017). https://doi.org/10.1103/PhysRevD.96.063007